

UNIVERSITEIT UTRECHT



INSTITUTE FOR SUBATOMIC PHYSICS

BACHELOR THESIS

**Study of the EMCal trigger bias on
the production of D^{*+} mesons in
proton-proton collisions at $\sqrt{s} = 13$
TeV in the ALICE experiment**

Adrianus Willem Voogt

supervised by
Dr. Alessandro Grelli
Dr. André Mischke

January 13, 2016

Abstract

In this thesis, the results for a simulation of the ALICE EMCal trigger bias on the production of D^{*+} mesons are presented. The implementation of EMCal triggers in pp $\sqrt{s} = 13$ TeV collisions was simulated by using PYTHIA 8.2 Monte Carlo simulations, producing a sample of 200 million events. Several triggers were considered, triggering exclusively on either electrons, photons or both, in combination with two trigger energy thresholds of 2 and 5 GeV. The EMCal trigger was simulated with an acceptance range of $|\eta| < 0.7$ and $0^\circ < \phi < 110^\circ$. The trigger bias was measured by calculating the enhancement factor for the yield of D^{*+} as a function of p_T , ϕ and η ; and by calculating the enhancement factor for the beauty fraction.

The 5 GeV electron trigger performs best when compared to other triggers: the trigger sample yields a general enhancement factor of 41 ± 1.3 . The 2 GeV electron trigger sample yields an enhancement factor of 30.5 ± 0.3 . The enhancement factor inside the EMCal ϕ and η acceptance range is significantly higher than outside this range. This leads to the conclusion that the trigger particles most frequently have their origin in the same fragmentation and decay chain as the observed D^{*+} meson.

In the high p_T limit, the 5 GeV electron trigger sample yields a maximum enhancement factor of $1.5146 * 10^6 \pm 1 * 10^3$. An enhancement in the beauty feed-down fraction of all D^{*+} is observed, from a fraction of 0.1077 ± 0.0003 for the minimum bias sample to 0.58 ± 0.03 for the 5 GeV electron trigger sample. The highest beauty enhancement is observed in the low p_T range, in the high p_T limit the beauty fraction in all trigger samples match the minimum bias beauty fraction.

A recommendation is made for the implementation of the 5 GeV electron EMCal trigger in the ALICE detector, because of its performance in the general enhancement of the D^{*+} yield; in the enhancement in the high p_T limit; and in the enhancement of the beauty fraction. The consequences of the trigger implementation, regarding the reduction in the amount of events, need to be determined in future studies.

Contents

1	Introduction	5
2	Theoretical framework	7
2.1	Standard Model	7
2.2	Quantum Chromodynamics	9
2.3	Quark-gluon plasma	11
2.4	Heavy-flavour quarks	12
2.5	D^{+*} and B mesons	14
2.6	Relevance of this study	15
3	Experimental setup	16
3.1	The ALICE detector	17
3.1.1	ITS	17
3.1.2	TPC	17
3.1.3	TOF	18
3.1.4	EMCal	19
3.1.5	Triggers	20
3.2	Analysis method	22
3.2.1	Pythia simulations	22
3.2.2	Root	23
4	Pythia Monte Carlo simulations	24
4.1	Monte Carlo simulations	24
4.2	Pythia configurations	24
4.3	Comparison of the minimum bias with HF forced data sample	26
4.4	Trigger implementation and event analysis	28
5	Trigger	30
5.1	Theoretical background	30
5.1.1	Functioning of trigger	30
5.1.2	Fragmentation and branching fractions	31
5.1.3	Trigger types	32
5.2	Electron trigger	33
5.3	Photon trigger	36

5.4	Combined trigger	38
5.5	Different Pythia configurations	39
6	Trigger bias on D^* yield	40
6.1	Minimum bias D^*	40
6.2	Overall enhancement	42
6.3	Trigger bias for ϕ and η distributions	43
6.4	Trigger bias for p_T distributions	47
7	Trigger bias on the beauty fraction	52
7.1	Beauty quark fraction	52
7.2	Trigger origin influence	53
7.3	D^* beauty fraction	54
7.4	B meson	60
8	Conclusions and outlook	61
A	Kaon trigger	65

Chapter 1

Introduction

The D^{*+} meson is of great importance to the ALICE collaboration. The meson can be a product of the fragmentation of either a beauty or a charm quark. This connection of the D^{*+} meson with charm and beauty quarks is important for the study of the quark-gluon plasma.

The goal of the ALICE collaboration is to investigate the quark-gluon plasma, a new phase of matter in which quarks and gluons are no longer confined in hadrons, but are free to travel in a much larger region. This quark-gluon plasma is of great importance to physicists, as it can teach them more about the strong interaction and the first moments after the Big Bang, when the universe is expected to have been filled with a quark-gluon plasma. The plasma can not be observed directly, as it only exists for a fraction of a second. However, the properties of the quark-gluon plasma *can* be studied indirectly, for example by sending probes into the plasma to observe their interaction. The ALICE collaboration has specifically designed the ALICE detector, located at the LHC at CERN, to study the quark-gluon plasma with state-of-the-art techniques. In the first moments of lead-lead collisions taking place inside the ALICE detector, a quark-gluon plasma is expected to form and subsequently to condensate into hadrons.

The charm and beauty quarks are designated by physicists as the best probes for the quark-gluon plasma. Those heavy quarks are produced in the first moments of the collision, simultaneously with the plasma. The charm and beauty quarks interact with the plasma, after which they hadronize into mesons we can detect. The D^{*+} meson, the subject of this thesis, is one of the possible fragmentation and decay products of the charm and beauty quarks. Because of the interaction of the charm and beauty quarks with the quark-gluon plasma, the properties of the resulting D^{*+} meson will also be influenced by that interaction. The quark-gluon plasma has left its ‘signature’ on the D^{*+} meson, which physicists can decipher. Therefore, it is of great importance for ALICE to detect the D^{*+} mesons produced in the collision, because they reveal something about the nature of the quark-gluon

plasma. D^{*+} mesons resulting from two types of collisions are compared: those produced in lead-lead collisions, where the quark-gluon plasma is expected to have been formed; and those produced in proton-proton collisions, where it has not been formed.

The objective for the study, done for this thesis, is to investigate a method which is expected to increase the D^{*+} meson yield in data sets from LHC collisions: the implementation of an EMCAL trigger. This device triggers on specific particles detected in a collision: energetic photons and electrons. For this thesis, the effect the implementation of this trigger has on the D^{*+} distributions is simulated. This effect is called the trigger bias. We expect the trigger to have a bias in the form of general enhancement of the D^{*+} yield, specifically for D^{*+} in the region of high transverse momentum. The theoretical reason and experimental results of this bias is presented in this thesis.

The first chapters clarify the theoretical background and experimental method for this thesis' study. In chapter 2, the theoretical background for this study is explained. The Standard Model, the strong interaction and the quark-gluon plasma are discussed, after which the importance of heavy-flavour quarks and D^{*+} mesons is made clear. In chapter 3, the experimental setup is discussed in two separate parts. First, the general experimental setup for ALICE is considered: the ALICE detector and the EMCAL subdetector are analyzed, along with an explanation of the functioning of an EMCAL trigger. Then, the specific experimental method for this study is discussed, by showing how I used Pythia and Root for the simulations. In chapter 4, the simulation program Pythia is discussed in more detail. The different Pythia configurations are compared, some preliminary results are discussed, in order to determine the quality of the simulation data, and the implementation of the trigger in the simulated collisions is explained.

In later chapters, the results of the trigger implementation are discussed. In chapter 5, the results for the trigger simulation are presented. The momentum distributions of the trigger particles are shown, and the performance of the trigger is considered in relation to the fraction of heavy-flavour decay trigger particles and the decrease in the amount of events. In chapter 6, the trigger bias on the D^{*+} yield is presented, both in general, and as a function of ϕ , η and p_T . In chapter 7, the trigger bias on the beauty fraction is presented. The enhancement of the ratio of D^{*+} from beauty decay is considered. Also, the trigger bias on the B meson yield is revealed.

In the conclusions and outlook, I summarize and interpret the results, along with recommendations for the implementation of the EMCAL trigger in the ALICE detector. Subsequently, I evaluate the methods used and the choices made in this study, in order to point out how future studies can improve or build upon the results of this thesis. In the appendix, some results for a kaon trigger are presented, functioning as an outset for future studies on the kaon trigger bias.

Chapter 2

Theoretical framework

In this thesis, we study the production of D^{*+} mesons. The main motivation for studying these mesons is their origin, which they have in charm and beauty quarks. These heavy quarks can act as probes for the quark-gluon plasma, as the interaction of the quarks with the plasma leaves its fingerprint on the observed properties of the quarks.

In this chapter, we will give a summary of basic theories in particle physics, in order to understand the theoretical motivation for this study. Specifically, we will have a limited discussion on the topics of Quantum Chromodynamics, the quark-gluon plasma, heavy-flavour quark production and heavy-flavour mesons.

2.1 Standard Model

The Standard Model of particle physics is the state-of-the-art model in this field, which is the result of elaborate research in the last decades. The Standard Model incorporates all known particles and interactions, except gravity. A schematic overview of all particles is given in figure 2.1. In the model, all particles are divided into three classes: quarks, leptons and gauge bosons. In addition to these three classes the Standard Model includes the Higgs boson: a unique particle, discovered in 2012 [2], that explains how certain elementary particles obtain their mass.

The leptons and quarks both consist of 6 particles and 6 corresponding anti-particles. These different quarks and leptons are called quark or lepton *flavours*. Both the particles and anti-particles are divided into three generations, with higher generations constituting heavier particles. The lepton class consist of the electron and the electron neutrino; the muon and the muon neutrino; the tau and the tau neutrino. The electron, muon and tau are charged particles, thereby capable of interaction through the electromagnetic force and the weak force, whereas all corresponding neutrinos are neutral and only capable of interaction through the weak force.

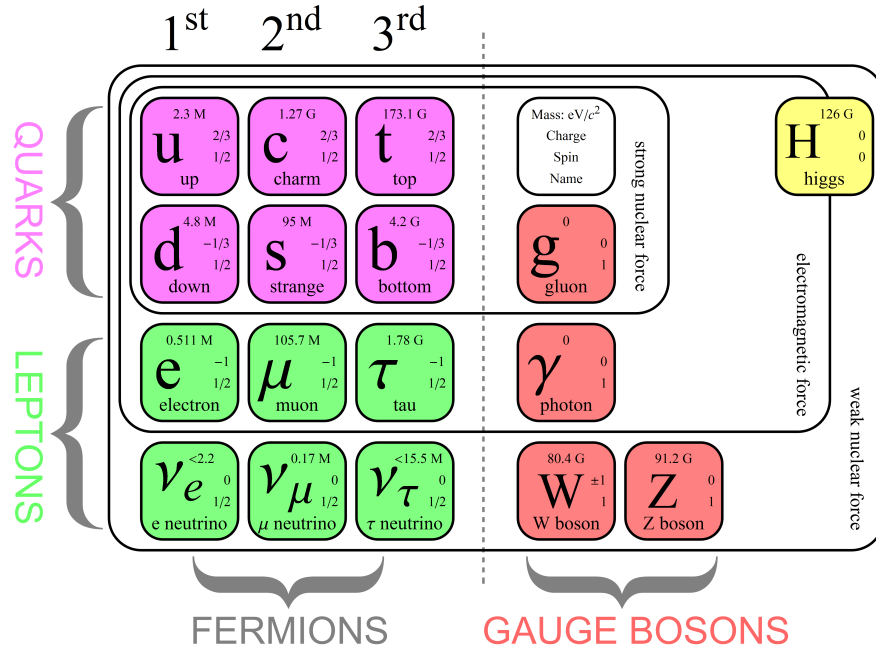


Figure 2.1: The Standard Model of elementary particle physics [1].

The quark class consists of the down and up quark; the strange and charm quark; the bottom and top quark. Our visible day-to-day environment is made up of the stable down and up quarks. The heavier quarks can be produced in particle accelerators, but will quickly decay into those first-generation quarks. However, for some experiments the quarks of higher generations can be useful. In this thesis, we are interested in the charm and bottom quarks. The bottom quark is also called the beauty quark, which is the name we will use from now on in this thesis.

Gauge bosons are force carriers, mediating all fundamental interactions between particles, except gravity. Gravity is a force which we observe at macroscopic level but we can neglect in particle physics. Remains the other three fundamental forces. The class consist of photons, mediating the electromagnetic force; W^+ , W^- and Z bosons, mediating the weak force; gluons, mediating the strong force. The electromagnetic force is the interaction between charged particles, described by quantum electrodynamics (QED). The weak force is, as the name suggests, a weak force, which is only present at small scales. It mediates the interactions between particles of different flavours. Together with the electromagnetic force, the weak force is described by the electroweak interaction. The strong force dominates at small scales, but is negligible at larger distances. It is described by Quantum Chromodynamics (QCD). Because of its relevance for this thesis we will discuss it more extensively in the next section.

2.2 Quantum Chromodynamics

The strong force is the most important interaction at small scales (in the range of a few femtometer). It gives stability to protons, neutrons and atomic nuclei as a whole. The strong force, described by Quantum Chromodynamics (QCD), constitutes the interaction between quarks and gluons, as they carry colour charge. The colour charge is a separate quantum number, which determines the way the strong force acts on the particle. This quantum number is not related to visible colours. There are three colours and three corresponding anticolours available: red, green, blue and antired, antigreen and antiblue. All colours, or a colour with its anticolour, mixed together produce a colourless or ‘white’ quantum state, which is the equivalence of a neutral state in quantum electrodynamics. All observable particles are colourless. This happens because coloured particles, such as quarks, are always observed together in bound states we call *hadrons*. There are two types of hadrons: the combination of three quarks, in all three different colours, called a *baryon*, and the combination of a quark with an antiquark (and thus a colour with its anticolour), called a *meson*. Apart from quarks, gluons too can carry colour charge. This means that gluons not only interact with quarks but can also interact with themselves, which is very different from QED, where photons do not carry charge and thus can not interact with other photons. Because of this capability of self-interaction, gluons are even capable of forming a bound state called a ‘glueball’. Evidence of glueballs being found has been provided recently [3]. These complications in QCD make the calculations more difficult than for QED, but also provide ways for new phenomena to be explained, such as quark confinement and asymptotic freedom.

Quarks confinement is the observation that quarks are always found together in a bound colourless state. When two quarks are pulled apart, the potential increases up to the point where it is energetically more favourable to create a new quark-antiquark pair, thereby forming a new meson. This mechanism is visualized in figure 2.2. When enough energy is available, a single quark may in this manner produce many hadrons clumped together, which is called a *jet*. This process of a single quark forming hadrons is called fragmentation or hadronization, and is not a well-understood phenomenon in particle physics.

Asymptotic freedom is the property in QCD that causes interaction between quarks to become asymptotically weaker as energy increases and distance decreases. This is thought to be caused by *antiscreening* of virtual gluons. In QED, virtual pairs of electrons and positrons in the vicinity of a charged particle polarize the vacuum, as the virtual particles of like charge are repelled and virtual particles of opposite charge are attracted to the charged particle. In effect, this screening partially cancels out the field of the particle at a finite distance. When the distance gets smaller, this screen-

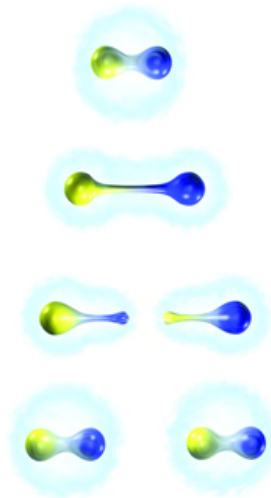


Figure 2.2: A graphical representation of one quark pair fragmenting into two mesons [4].

ing effect gets weaker. In QCD, the opposite mechanism happens, which is therefore called antiscreening. The gluons surrounding a quark carry themselves a colour charge, thereby enhancing the net colour charge of a quark. When the distance to the quark is smaller, the antiscreening effect is diminished. In confined states, the quarks are so close to each other that their interaction is very weak. The quarks bound in a hadron state are therefore said to be asymptotically free.

This qualitative explanation of asymptotic freedom by the mechanism of antiscreening does not fully cover the mathematical description. The interaction strength is not truly dependent on the distance, but on the exchanged momentum. In QCD calculations, the interaction strength is determined by the coupling constant. This coupling constant is however not always constant, as it can depend on the energy scale. This dependence of the coupling on the energy scale is known as *running* of the coupling. For QCD, the coupling can approximately be described with equation 2.1.

$$\alpha(k^2) \approx \frac{1}{\beta^0 \ln(k^2/\Lambda^2)} \quad (2.1)$$

In this equation, α is the coupling as a function of k , β and Λ are constants and $k = \frac{2\pi}{\lambda}$ is the wavenumber, through $\lambda = \frac{h}{p}$ related to the momentum of the particle. We observe in this equation that the effective coupling constant decreases with energy, leading to asymptotical behaviour at high energies [5]. Normally, this asymptotic behaviour for quarks occurs inside the bound states of hadrons. However, if we increase the energy or

density scale, we will observe a phase transition as the asymptotically free quarks are not confined anymore in the hadron state. We call this new phase a quark-gluon plasma.

2.3 Quark-gluon plasma

The quark-gluon plasma (QGP) is a new phase of matter in which quarks and gluons behave as asymptotically free particles in a much larger volume than a hadron. This phase is theorized to occur at extremely high energies or densities. In fact, this phase would have occurred only in the first moments of the universe, a few microsecond after the Big Bang [6]. The study of the QGP is therefore essential for the understanding of the early universe. In figure 2.3 we see a phase diagram for the different energy and density scales in the QCD theory. At low temperatures and densities the quarks are confined in hadrons, the state which constitutes ordinary matter. At high densities, but low temperatures, a 1st-order phase transition is expected to lead to the formation of a QGP, as for example within neutron stars. At high temperatures and low densities, a QGP is also formed without going through a 1st-order phase transition. In this region of density and energy, we find similar conditions as in the early universe. Apart from helping to understand the early universe, the QGP is also the perfect study case for verification of QCD theories about behaviour of coloured particles at high temperature.

In state-of-the-art particle accelerators such as the LHC in CERN, the QGP is expected to be formed when two energetic lead-ions are collided. Due to relativistic length-contraction, the lead-ions form thin discs, which then collide at center-of-mass energies of currently 5.02 TeV per nucleon pair [7], trespassing the 1 PeV for the total center-of-mass energy [8]. At the moment of impact, the temperature is high enough to deconfine the quarks, thus forming a QGP. The plasma then starts to expand very fast, cooling down to the point where the quarks are again confined into hadrons.

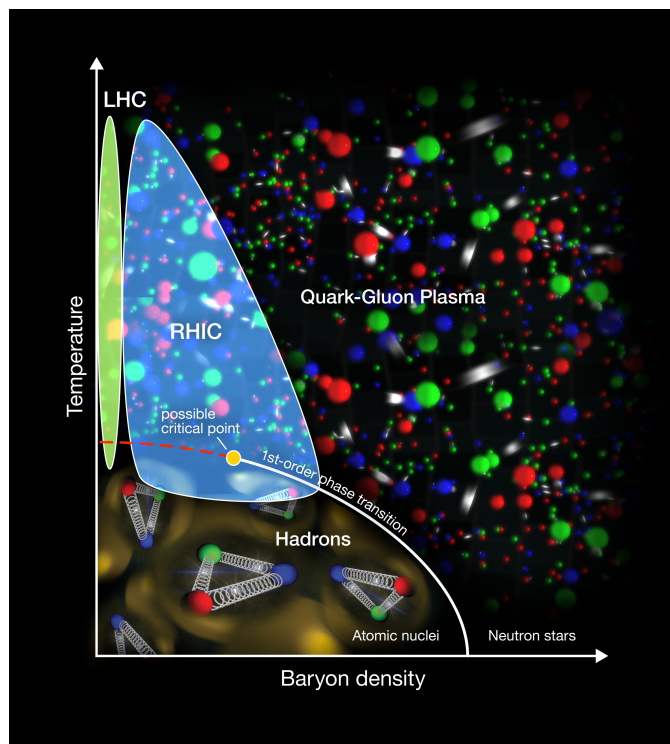


Figure 2.3: A phase diagram for matter in different energy and density regions, according to QCD [9].

2.4 Heavy-flavour quarks

Because the QGP cannot be detected directly, we must use probes to learn more about its properties. Good candidates for a QGP probe are heavy-flavour (HF) quarks, specifically charm and beauty quarks. These HF quarks are created before or simultaneously with the formation of the QGP. Heavy quarks mainly come from the colliding of two gluons: in that case the gluons form a heavy quark-antiquark pair. The production time of these heavy quarks is proportional to $1/m_q$ where m_q is the mass of the quark [10]. In this way, heavier quarks are good probes for the QGP, as they are produced before the QGP and then travel through the expanding plasma. Because those heavy quarks are coloured particles, they experience strong interaction with the plasma. While travelling through the plasma, the HF quarks radiate gluons¹. The radiation of gluons will be suppressed below a certain angle $\theta < \frac{m_q}{E_q}$ which is dependent on the quark mass [11]. This mechanism, known as the dead-cone effect, causes heavier quarks to lose less energy in the form of gluon radiation. This enhances the probability that fragmentation of this

¹Just as electrons radiate photons in an electromagnetic field, a mechanism which is called Bremsstrahlung.

quark forms a meson with high enough energy to be reconstructed through its decay products.

The top quark is the heaviest, but also the most unstable quark. The top quark has an extremely short average lifetime of $5 * 10^{-25}$ s. Therefore, the top quark decays too quickly to be used as a QGP probe [12]. This leaves the charm and beauty quarks as the best probes for the QGP, from now on referred to as HF quarks. How we do investigate the properties of the QGP by capturing HF quark products? By comparing the properties of those particles in collisions where a QGP was formed, with the properties in collisions where no QGP was formed. In order to do this, we need to go through a couple of steps.

HF quarks can not be observed directly, so the fragmentation products need to be measured instead. First of all, mesons resulting from the hadronization of HF quarks (referred to as HF mesons) are reconstructed by analyzing their decay products. The properties of these mesons are closely related to the properties of the HF quarks from which they are fragmentation products. The yield, energy and transverse momentum² (p_T) of the mesons is measured. Then, the meson yield as a function of p_T is compared for two situations: when a QGP has been present in the collisions, e.g. in lead-lead collisions; and when a QGP has not been present, e.g. in proton-proton collisions. However, this comparison between the two types of collisions is not straightforward, as lead-lead (Pb-Pb) collisions have a different center-of-mass energy, more nucleons are present and the ions do not overlap completely. These effects taken into consideration, the result for this comparison is the nuclear modification factor as given in equation 2.2.

The nuclear modification factor is the ratio of the derivative of the yield to p_T in Pb-Pb collisions over the derivative of the yield to p_T in pp collisions, normalized for the amount of nucleons in the collision. In equation 2.2, N_{AA} is the normalised yield measured in heavy-ion collisions; $\langle T_{AA} \rangle$ is the average nuclear overlap function (which tells how many nucleons on average participate in the Pb-Pb collisions, as the ions do not necessarily collide head-on); and $d\sigma_{pp}$ is the production cross-section for the meson in pp collisions [13].

$$R_{AA}(p_T) = \frac{dN_{AA}/dp_T}{\langle T_{AA} \rangle d\sigma_{pp}/dp_T} \quad (2.2)$$

This nuclear modification factor is an observable of the QGP, as it describes how the yield of HF mesons versus the p_T is changed under influence of the presence of the QGP. When the QGP is not present, R_{AA} should be 1. In this case, the Pb-Pb collision is approximately a superposition of many pp collisions, no different physics is involved. When the QGP is present,

²The momentum component perpendicular to the beam line, as to remove the momentum which might have remained from before the collision.

the factor will be smaller than 1, as the HF quark loses energy as it travels through the plasma. In this case, the R_{AA} value, as a function of p_T , gives information about the interaction of the HF quarks with the QGP, thus about the properties of the plasma itself.

2.5 D^{+*} and B mesons

The best candidates as probes for the QGP are charm and beauty quarks. After travelling through the QGP, the HF quarks hadronize into HF mesons, which can then be detected. There are several possible mesons into which a charm or beauty quark can hadronize: the D^+ , D^0 , D^{+*} and more for the charm, with their charge conjugates for the anticharm; the B^+ , B^0 , B^{+*} and more for the beauty, with their charge conjugates for the antibeauty. Because its reconstruction is easiest of all frequently present charm mesons, the D^{+*} meson is chosen for most studies on HF decays and QGP probes. The D^{+*} is an excited state of a charm and antidown quark ($c\bar{d}$) and for the antiparticle the D^{-*} , ($\bar{c}d$). For this study we don't distinguish particles from their antiparticles, so from now on in this thesis we will refer to both the D^{+*} and D^{-*} by D^* .

The D^* can be produced directly by fragmentation of a charm quark (called prompt D^*) or from the decay of a B meson (called B feed-down D^*). This B meson is a product of the fragmentation of a beauty quark. Therefore, a D^* can be a product of either a charm or a beauty quark, which we will an important feature for this thesis. Because of its higher mass, a beauty quark is more rare in a collision than a charm quark. However, a beauty quark is produced earlier and loses less energy through gluon radiation (see previous section). In this way a beauty quark is regarded as a better probe for the QGP. In future studies, it might be possible to distinguish prompt D^* from feed-down D^* in order to study the nuclear modification factor for beauty quark products only. In this thesis, therefore, it is relevant to include a distinction between prompt D^* and feed-down D^* , also called charm and beauty produced D^* .

Although a D^* meson can not be detected directly, the presence of a D^* can be signified by other, observable, particles: the decay products of the D^* . First, these decay products help in the reconstruction of the D^* mesons after the collisions is recorded. The meson can be reconstructed by analyzing the trajectories of its decay products and implying topological cuts in order to remove background. Second, early detection of the decay products can function as a real-time trigger on the collisions, in order to select interesting collisions to be recorded. The second use of decay products, signifying the presence of D^* mesons, is used in this study.

The trigger of interest is the EMCAL trigger, which triggers on electrons³

³In this thesis, positrons are included when mentioning electrons.

and photons. Implementation of the EMCAL trigger means, that only those collisions are detected, in which an energetic electron or photon has been found. In order to understand why we examine this trigger, we must consider the relation of electrons to D^* mesons. B mesons can decay into a D^* through the following decay channel: $B \rightarrow D^{*+} + e^- + \bar{\nu}_e$, including all charge conjugates. Also, the D^* itself can decay through the following decay channel: $D^{*+} \rightarrow X + e^+ + \nu_e$, including all charge conjugates. In this way, the presence of a D^* can be indicated by an electron. Moreover, because of the high mass of the D^* meson, the associated electron will be very energetic. Because of the strong connection between energetic electrons and D^* mesons, the EMCAL trigger is potentially a very powerful tool to enhance the D^* yield. The relation of the D^* with photons is more difficult to determine, but the expectation is that D^* are not signified by photons as much as by electrons. The relation of the D^* with the trigger particles is further discussed in chapter 5. The mechanism of the EMCAL trigger is further discussed in chapter 3.

2.6 Relevance of this study

This thesis presents the results of the EMCAL trigger bias on the yield of D^* mesons. What I want to address here is the connection of the thesis with the theoretical framework explained in this chapter and the current state of the studies about the QGP.

As we have discussed in this chapter, we want to investigate the QGP by using HF quarks as a probe. These HF quarks are measured indirectly, by reconstructing the D^* mesons into which they might have hadronized. The yield of these D^* is compared, as a function of p_T , for Pb-Pb collisions and pp collisions by calculation of the nuclear modification factor (equation 2.2). In order to help obtain a good result for the nuclear modification factor, we have three separate goals which are addressed in this thesis by analyzing the effect of an EMCAL trigger.

1. General increase in the D^* yield, in order to have better statistic for the calculation of the nuclear modification factor.
2. Specific increase in the yield of D^* with high p_T , in order to have better statistic in this high p_T region.
3. Increase in the fraction of feed-down D^* , or the beauty fraction in general, as to help future studies calculate the nuclear modification factor for beauty separately.

Chapter 3

Experimental setup

The study for this thesis is done with the simulation software Pythia, but we first need to understand what precisely is simulated. In this chapter, therefore, we first discuss the ALICE detector located at CERN. Then, we consider the software used for the study of this thesis.

CERN, the European Organization for Nuclear Research, is an internationally renowned center for particle physics. At CERN, physicists reveal the fundamental principles of our universe, by observing the properties of matter at extremely high energies. These high levels of energy are achieved by accelerating protons or lead-ions to near the speed of light, after which the particles collide, releasing huge amounts of energy. This is done at the Large Hadron Collider (LHC), the most powerful particle accelerator in the world, located deep beneath the ground at the French-Swiss border.

The LHC facilitates two types of collisions relevant for this thesis. The first type is the collision of two protons (pp collision), currently at a center-of-mass energy of $\sqrt{s_{pp}} = 13$ TeV. The second type is the collision of two lead-ions, currently at a center-of-mass energy of $\sqrt{s_{NN}} = 5.02$ TeV per nucleon pair [7]. Because lead-ions consist of many nucleons, the total amount of energy in the center-of-mass frame is much higher. The energy values for these types of collisions are expected to be increased in future LHC runs.

The collisions in LHC are registered by different detectors, located at different points in the accelerator. These detectors stand for different experiments, each of which is focused on a specific area of particle physics. There are currently four main experiments in the LHC, in a total of seven experiments: ATLAS, LHCb, CMS and ALICE. This thesis is done for the ALICE collaboration and will therefore discuss the ALICE detector.

3.1 The ALICE detector

ALICE stands for A Large Ion Collider Experiment. The goal of ALICE is to study the physics of strongly interacting matter at extremely high energies, where the formation of the QGP is expected. Both proton-proton and lead-lead collisions are analysed, as to compare the results of the particle interactions in these two energy regions. In proton-proton collisions, the QGP is not expected to be present.

After the LHC accelerated the protons or ions and made them collide in the center of the ALICE detector, the produced particles - which could be anything from common particles e.g. photons, electrons or pions, to rare particles e.g. charm and beauty hadrons - are traced and their properties measured in the various parts of the detector. In order to identify the particles and measure their momentum, the ALICE detector makes use of different subdetectors.

The ALICE detector is schematically shown in 3.1. The main element of the ALICE detector is the central barrel, optimized for detecting photons, electrons and hadrons. The central barrel is embedded in a solenoid magnet producing a magnetic field strength of 0.5 Tesla, in order to bend the trajectories of the particles. The detector covers the pseudorapidity range of $|\eta| < 0.9$. The pseudorapidity η is a spatial coordinate describing the angle relative to the beam axis. Its usage is preferred over using the polar angle θ , as η is Lorentz invariant. The range of $|\eta| < 0.9$ is about the same as a polar angle of 90° : $45^\circ < \theta < 135^\circ$. Particles outside this η range cannot be detected. As for the azimuthal angle ϕ , ALICE covers the full range. In the next sections, the for this thesis relevant subdetectors of ALICE will be discussed.

3.1.1 ITS

The Inner Tracking System (ITS) is a silicon detector, cylindrically shaped around the collision point, which is called the primary vertex. The ITS consists of six layers including a Silicon Pixel Detector (SPD), a Silicon Drift Detector (SDD) and a Silicon Strip Detector (SSD). The layers are placed at a radial distance between 3.9 and 43 cm from the beamline: it is the first detector the produced particles pass through. When the particles pass through the silicon cells, a small ionizing current is measured. The signals of all layers together can reconstruct the trajectory of the particle. The ITS is mainly used for locating the primary vertex and tracking produced particles.

3.1.2 TPC

The Time Projection Chamber (TPC) is a cylindrical chamber filled with a Ne/CO₂ gas mixture, placed in an electrical field. Charged particles travel-

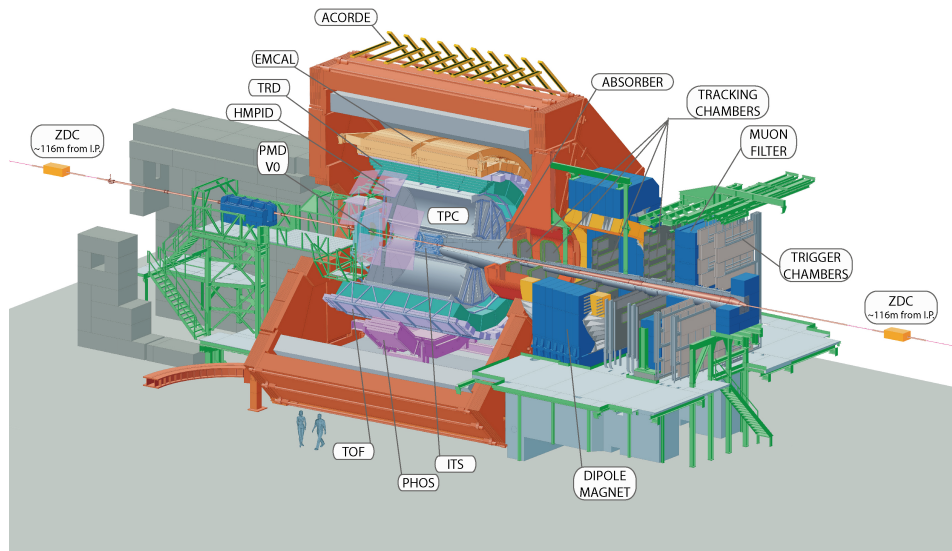


Figure 3.1: A schematic view of the ALICE detector [14].

ling through the TPC ionize the gas along their path. The electrons resulting from this ionization are accelerated to a detector. When the points of impact of these electrons are analyzed, the trajectory of the charged particle is reconstructed. Besides the trajectory, the energy loss per distance ($\frac{dE}{dx}$) and momentum is measured. The energy loss per distance versus momentum is a characteristic function, distinct for every type of charged particle. These characteristic functions are observed as bands in figure 3.2. These two properties are therefore used to identify the particle. The TPC is therefore capable of tracking, momentum measurement and particle identification. The particle has to be charged, however, to be registered by the TPC.

3.1.3 TOF

The Time Of Flight subdetector consists of a stack of resisting glass plates. Just like in the TPC, a charged particle will ionize the gas in between. The ionization current is amplified and measured at the resistive plates. The TOF measures the time that the particle needs to travel from its vertex to the TOF. Together with the momentum measurement and the track length, this time interval determines the type of particle, as testified by the different bands in figure 3.3. When the TOF data is combined with the TPC and ITS data, reliable identification of the particle can be achieved.

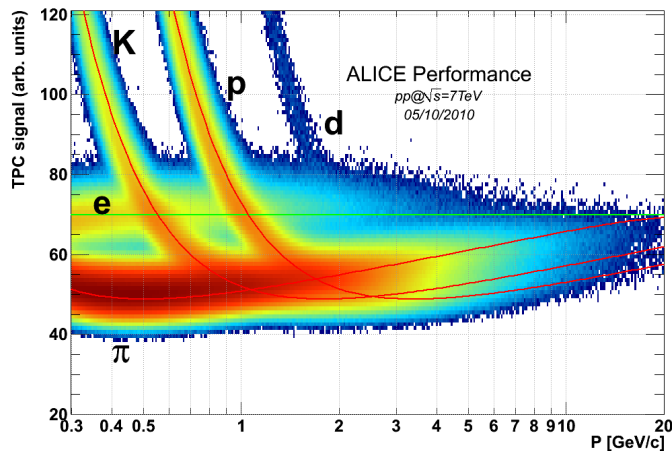


Figure 3.2: Diagram produced by the TPC detector, showing $\frac{dE}{dx}$ as a function of momentum p . The bands are characteristic for the particles π^+ , K^+ , p , d and e^- , including all their charge conjugates [15].

3.1.4 EMCal

The electromagnetic calorimeter (EMCal) detector is an important sub-detector in ALICE for this thesis. The EMCal is the detector which would be used for the triggers studied in this thesis. The EMCal is located at a radius of 4.6 m from the beam line and has a different range in spatial coordinates than the rest of the ALICE detector. The general ALICE detector covers a pseudorapidity range of $|\eta| < 0.9$ and the full range of the azimuthal angle ϕ . The EMCal however, covers a pseudorapidity range of $|\eta| < 0.7$ and a range in the azimuthal angle of $0^\circ < \phi < 110^\circ$. In figure 3.4 the location of the EMCal in the full ALICE detector is shown from the side, along with other subdetectors. The limited ϕ range of the EMCal is clearly visible.

The EMCal consists of almost 13,000 individual lead-scintillator towers. These towers are embedded in Super Modules, which together form the continuous arch of the total EMCal detector. The EMCal arch, composed of the Super Modules, is shown in figure 3.5. Particles, while travelling through the towers filled with lead plates, deposit all their energy in the towers. This energy is measured, and combined with the data of the other detectors, this give the original energy of the particles. The typical shape of a shower the particle produces inside the EMCal towers, can help discriminate between the different particles, such as photons, pions and electrons. How the EMCal can be used for triggering, will be explained in the next section¹.

¹More information about the EMCal can be found at the EMCal performance report [17].

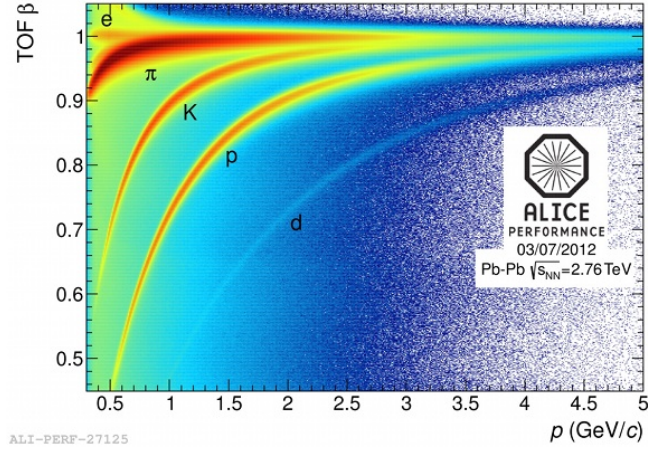


Figure 3.3: Diagram produced by the TOF detector, showing $\beta = \frac{v}{c}$ as a function of momentum p . The bands are characteristic for the particles π^+ , K^+ , p , d and e^- , including all their charge conjugates [16].

3.1.5 Triggers

Collisions in ALICE are expected to occur 400,000 times a second for pp collisions and 4,000 times a second for Pb-Pb collisions. However, the quality of these collisions is not constant. For example, several collisions can pile up in the detector, producing bad data samples. The collision quality has to be evaluated before the detector records the event, to avoid huge piles of useless data. Besides, the ALICE detector can only safely record 500 collisions per second [17], because of the time the TPC needs to restore the equilibrium state. Because of this, only a fraction of all collisions can be recorded anyway. To tackle these issues, the ALICE detector uses triggers. Triggers are mechanisms that give a signal to the full detector to start recording the collisions, only if certain trigger conditions are met. These conditions vary for the different trigger used. In this way, triggers make the decision whether the collision is worth saving or not.

In normal ALICE data sampling, a hierarchical system of three trigger is used: L0, L1 and L2. The L0 is the most important type, as it triggers on the most basic conditions. For example: the condition that the subdetectors (especially the TPC) and the data acquisition system are not busy. The L1 and L2 triggers impose the condition that there is no pile-up of collisions in the detector, which would be the case if subsequent collisions are too close to each other. The normal ALICE triggers therefore only make sure that the recorded collisions result in correct events, suitable for data analysis. They do not trigger on the type of particles produced in the collision. This type of data sampling, using only the L0, L1 and L2 triggers, is called *minimum bias* sampling. This configuration of the ALICE detector is not expected to

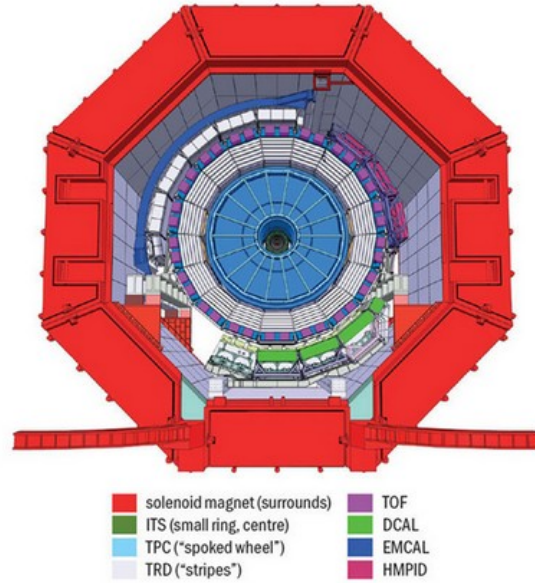


Figure 3.4: Schematic sideview of the ALICE detector with some subdetectors. The limited range of the EMCal (blue) in ϕ is clearly visible [18].

have any bias on which particles are present in the recorded collision.

It is possible to impose additional triggers on the normal L0, L1 and L2 triggers. These additional triggers can be used to filter collisions, which are valuable for certain studies. In this thesis, we study the effect that imposing an EMCal trigger would have on the produced data. The EMCal is designed to detect electromagnetic particles, i.e. photons and charged particles, and to measure their energy. This detector can therefore be used as a trigger on those particles. The appropriation of the EMCal as a trigger device would mean, that the EMCal gives a signal to the detector to record a collision, only if a particle above a certain energy threshold is measured, in one of the towers of the EMCal. This particle could be a photon, an electron (or positron) or even a charged hadron. In this thesis, we mainly discuss the electron and photon EMCal trigger. The reason for this is the relation energetic electrons and photons have with HF quarks and the D^* meson. The energy threshold can be set to any value, in this thesis two values are considered: 2 and 5 GeV. We expect this trigger to have a bias on the yield of certain particles. Specifically, particles associated with energetic photons and electrons are expected to be found more frequently in data samples obtained using the EMCal trigger. In contrast to minimum bias samples, the collision data samples obtained using an EMCal trigger are in this thesis called *trigger samples*.

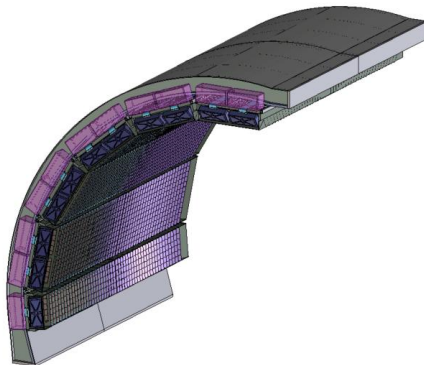


Figure 3.5: Schematic image of the full EMCal detector. The individual lead-scintillator towers are visible, which are embedded in the Super Modules. [19].

3.2 Analysis method

This thesis is about simulating the implementation of an EMCal trigger in the ALICE detector. The analysis software used for this simulation is discussed briefly in this section. In the next chapter, I will explain in detail how the results, presented in this thesis, were obtained.

3.2.1 Pythia simulations

The data set for this thesis is obtained using the simulation software PYTHIA 8.2. This program is designed to simulate high-energy collision events, such as the collisions in the LHC. The simulation involves the application of complex models of physics, including results from QCD and electroweak theory. PYTHIA 8.2 is written in C++, while former versions were written using Fortran.

Simulation software, such as Pythia, is helpful for physicists, because it can provide results for hypothetical situations, which can not be configured in real-life experiments; because it can make predictions for future experiments; or because it enables data from real experiments to be compared with current theoretical models in physics. In this study, the simulation is done in order to get an expectation of the effect of the implementation of an EMCal trigger on D^{*+} production. In order to achieve this goal, collisions like those in ALICE were simulated, producing a data set of 200 million collisions, which are subsequently called *events*. All particles that are produced, from the quark level up to the level of hadrons and their decay products, are saved along with their properties like energy, momentum, Particle Identification (PID) code, values in η and ϕ , and a reference to their origin and their decay products. The simulated events were later analyzed using the Root

framework. The Pythia simulation does not include the interaction of the particles with the ALICE detector. An improvement of the data presented in this thesis, can therefore be obtained by applying a program like GEANT. GEANT provides tools to model the effect of the ALICE detector on the particle production and yield. In the next chapter, we will have a more detailed discussion of Pythia and how it was applied in this study.

3.2.2 Root

After Pythia was used for simulating collisions and recording all particles, the triggers were applied and the data analyzed using Root. Root is an object oriented data analysis framework written in C++. It is originally designed by René Brun and Fons Rademakers in 1995. It is the most used method of data analysis by particle physicists. Root essentially consists of a hierarchy of classes, libraries and modules. The common base class is *TObject*; the classes most used for this study are *TH1* and *TF1*, for the construction of histograms and mathematical functions.

Root was used to filter trigger events in the collisions Pythia produced. This was done by labelling collisions that met the trigger conditions as ‘trigger events’. This yielded different data samples: a minimum bias sample and several trigger samples, which are subsamples of the minimum bias sample. Subsequently, relevant particles were searched for in the various data samples and their properties were stored in histograms. These histograms then provided information about the distribution of certain properties (e.g. transverse momentum) for certain particles (e.g. electrons or D* mesons) in a specified data set (e.g. the 5 GeV electron trigger sample). We will discuss in detail the implementation of the triggers and related functions in the next chapter.

Chapter 4

Pythia Monte Carlo simulations

In the last chapter we discussed the details of the LHC collisions, the ALICE detector and the trigger mechanism. It was also mentioned that as analysis method for this thesis, the simulation program Pythia and the data analysis program Root were used. In this chapter, we will discuss how the collision events were simulated in Pythia. We will compare different Pythia settings and look at the agreement of the different configurations. The implementation of the trigger and event analysis will be explained in the last section.

4.1 Monte Carlo simulations

PYTHIA 8.2 is a simulation program which works with the Monte Carlo technique. This technique produces random data points in a defined mathematical domain, according to a defined probability distribution in that domain. These produced data point are then used for deterministic calculations which eventually give the final result for one event. This process is generally repeated for a huge number of events, to counter probabilistic fluctuations.

In the case of Pythia, the mathematical domain and probability distribution are calculated using the laws of Quantum Chromodynamics and other sophisticated areas of physics. With this Monte Carlo technique, Pythia is able to produce realistic collision events, where the user can choose the type of collision and the specific interactions involved. For this thesis, Pythia produced proton-proton (pp) collision events at a center-of-mass energy of 13 TeV, to simulate current 2015 pp collisions in ALICE in the LHC.

4.2 Pythia configurations

A user of Pythia can choose between many different configurations, which determine the type of collision events that Pythia will produce. For this thesis,

we compare two configurations called HF forced and minimum bias. They both have in common the configuration of producing pp collision events at 13 TeV. However, they differ in the production of heavy-flavour quarks. The HF forced configuration makes Pythia produce collisions with the condition that in every event, a heavy-flavour (charm or beauty) quark is present. This does not mean that in every event a charm *and* a beauty quark are present, because that would distort the charm over beauty ratio, which would not result in a good sample for the analysis. It does mean that we are certain to find a charm *or* a beauty quark in one event, but that the probability of finding a charm is that much higher than finding a beauty, that in the end the charm over beauty ratio will be in agreement with real LHC collisions. Below are the specific Pythia settings used for the HF forced configuration.

HF forced

- HardQCD:gg2bbbar = on
- HardQCD:qqbar2bbbar = on
- ParticleData:mbRun=4.75
- HardQCD:gg2ccbar = on
- HardQCD:qqbar2ccbar = on
- ParticleData:mcRun=1.25
- BeamRemnants:primordialKT=on
- BeamRemnants:primordialKTsoft=0
- BeamRemnants:primordialKTthard=2.03
- BeamRemnants:halfScaleForKT=0
- BeamRemnants:halfMassForKT=0

The minimum bias sample has no such condition placed on the produced particles. Therefore, in many events a HF quark will not be present. Only a small part of a minimum bias sample will give D* mesons, the part we are interested in. However, a minimum bias sample will be the sample that is most in agreement with a real ALICE data sample, as nature itself is not supposed to have a bias. Below is the setting used for the minimum bias configuration. In the next section, we will compare the two configurations to decide which one to use.

Minimum bias

- SoftQCD:all=on

4.3 Comparison of the minimum bias with HF forced data sample

The HF forced Pythia configuration results in more D^* mesons in the same number of events. For this thesis, there was a time limit for the simulation process, placing a limit on the amount of events that could be produced. In order to obtain as much statistic as possible, it therefore would be a good choice to go for the HF forced setting with more D^* per event. However, the results also have to be in accordance with reality in order to be useful at all. It has to be checked if the HF forced setting results are in accordance with the realistic minimum bias setting. In order to make a choice for one of the Pythia settings, we therefore have to compare their resulting distributions.

In figure 4.1 we compare the p_T distributions of the D^* produced with the two Pythia configurations. In the same number of events we see a huge difference in the amount of D^* mesons: $1.05 \cdot 10^6$ for HF forced versus $1.52 \cdot 10^5$ for minimum bias. This difference is in agreement with our expectation, more HF quarks cause more D^* in the HF forced sample. However, we also observe a difference in the shape of the p_T distribution. This difference is seen in the right panel: at low p_T the amount of D^* is enhanced the most. Around $p_T = 2 \text{ GeV}/c$ we observe the maximum enhancement with an increase of a factor of 10. At high p_T , the enhancement is much less, about a factor of 3. This means that HF forced not just increases the amount of events with D^* , but it also shifts the p_T distribution of the produced D^* . This shift will influence the triggering process by suppressing the chance that a sufficiently energetic electron will be found *per* D^* meson.

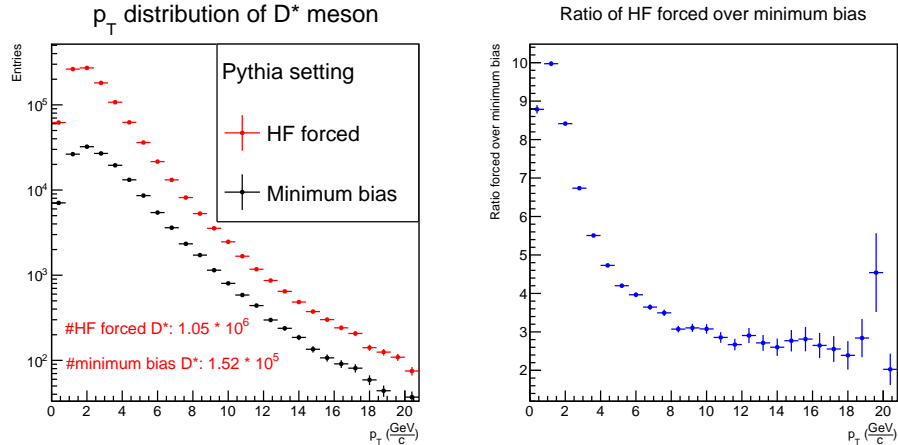


Figure 4.1: D^* transverse momentum distribution with minimum bias and HF forced Pythia configurations. Left panel: both p_T distributions. Right panel: ratio of HF forced over minimum bias. The amount of collision events is the same for these two configurations (20 million events).

4.3. COMPARISON OF THE MINIMUM BIAS WITH HF FORCED DATA SAMPLE 27

In figure 4.2 we observe the p_T distributions of the electrons produced with the two Pythia configurations. Also here, there is an increase in the amount of electrons in the HF forced sample. However, this increase is much less (factor of 1.3 more) than the increase in the amount of D^* (factor of 6.9 more). While D^* can only have their origin in HF quarks, electrons can be an offspring of many other particles as well. This means that, besides in events with HF quarks, there will also be many electrons present in events without HF quarks. In the right panel we see the ratio of the two distributions and we learn that especially electrons with high p_T are enhanced in the HF forced sample, which agrees with our expectation of electrons from HF decays being more energetic.

From the electron distributions we can conclude that electrons are enhanced in the HF forced sample. However, they are enhanced by only a small factor. This means that, in the minimum bias sample, there must be many electrons with their origin *not* in HF decays. These *background* electrons in the minimum bias sample will distort the trigger mechanism, which in the HF forced sample is only influenced by electrons coming from HF decays. In chapter 5 we will further discuss the electron distributions and the effect on the trigger.

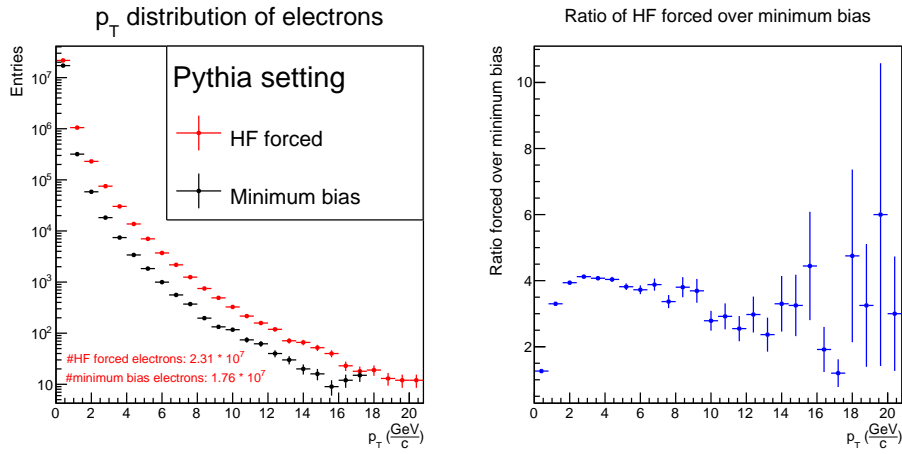


Figure 4.2: Electron transverse momentum distribution with minimum bias and HF forced Pythia configurations. Left panel: both p_T distributions. Right panel: ratio of HF forced over minimum bias. The amount of collision events is the same for these two configurations (20 million events).

In figure 4.3 we see the enhancement factor for the D^* as a function of the p_T of the D^* . How this enhancement is calculated will be explained in chapter 6. What is important for now, is the different shape of the enhancement plot for both Pythia configurations. Both for the photon and the electron trigger the enhancement is very different for the two configurations. With

the results of the D^* and electron p_T distributions in mind, we could have expected that the trigger mechanism gives a completely different result for the D^* enhancement in both configurations. The enhancement is not only shifted vertically, the shape is also different as we can observe from the ratio of the two configurations, plotted in the right panel.

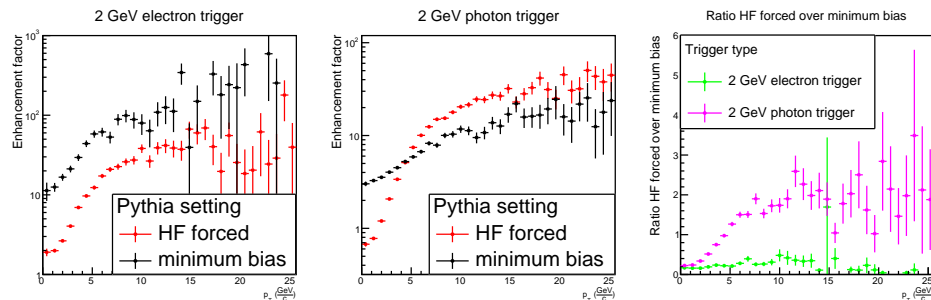


Figure 4.3: Enhancement for the D^* against p_T with minimum bias and HF forced Pythia configurations. Left panel: for the 2 GeV electron trigger. Middle panel: for the 2 GeV photon trigger. Right panel: ratio of the enhancement from both Pythia configurations, for the 2 GeV electron and photon trigger.

Using all previous results, we make a choice between the two Pythia configurations. We see that the important distributions in both samples are not in agreement with each other. The HF forced sample would give us more D^* and more statistic with the same number of events, but the minimum bias sample will be most realistic. I originally chose for the HF forced setting to have as much statistic, but as the distributions and, most importantly, the enhancement turned out to be incompatible with the minimum bias sample, and therefore real ALICE collisions, this was not a viable option anymore. All results in this thesis, unless stated otherwise, will therefore be from a minimum bias sample.

For this thesis, a sample of 200 million pp collisions at $\sqrt{s} = 13$ TeV was used.

4.4 Trigger implementation and event analysis

We discussed the basic configurations in Pythia for producing events, but more had to be done in order to obtain the results. Here the implementation of the trigger mechanism and the analysis method in the code will be explained.

After Pythia has been initialized by implementing the basic configurations and started producing events, we simulate the effect of a trigger. Instead of only observing or keeping events which produced a trigger signal, as ALICE does when the trigger mechanism is turned on, Pythia keeps all

events. Therefore, the trigger is implemented in the following way. A first round of analysis would search through all particles in a produced event, and when a particle was found that matched the criteria for a specific trigger, that event would be flagged as a trigger event for the relevant type of trigger. For example: an event with a 7 GeV photon coming from a charm decay, and found within the EMCal acceptance range, being $|\eta| < 0.7$ and $0^\circ < \phi < 110^\circ$, would be flagged as a trigger event for the following trigger types. These different triggers will be explained in chapter 5.

- 5 GeV charm photon trigger
- 2 GeV charm photon trigger
- 5 GeV photon trigger
- 2 GeV photon trigger
- 5 GeV electron and photon trigger
- 2 GeV electron and photon trigger

After this first round of analysis, in a second round all particles in the event are scanned, to find HF quarks, D^* and B mesons. When found, particle information such as the values of η , ϕ or p_T , would be put into different histograms according to the type of event (trigger event or not), to the value of η (in the range of the detector $|\eta| < 0.9$ or outside) and, for the D^* , the origin (charm or beauty) and the decay channel (decay into observable particles or other channels).

This origin and decay analysis has to be explained a little further. For a specific particle, Pythia remembers the so called *mother* and *daughter* particles in the event. A mother is the particle which decayed (or fragmented) into the examined particle, a daughter is a particle into which the examined particle decayed. In order to know if a D^* , electron or photon came from a charm or beauty quark, we can inspect the mothers of the particle. If the direct mother would be another hadron or lepton, the program would further inquire into the mother of the mother etcetera, until a charm or beauty quark was found. Then the examined particle would be flagged as *from charm* or *from beauty* and simultaneously for both as *from heavy-flavour*. In order to find the decay channel, there would be the same analysis for the daughter particles. If the meson was found to have decayed into the desired particles, the meson would be flagged as *decayed through desired channel*.

The result of this analysis would be a file containing many histograms, each of which would give a η , ϕ or p_T distribution for very specific types and very general types of D^* mesons and other particles.

Chapter 5

Trigger

In chapter 3 I have discussed in detail the mechanism of the EMCal trigger. In chapter 4 the implementation of the trigger in the Pythia simulations has been explained. In this chapter, the details of the trigger simulation will be further explored. First, we discuss the function of the trigger in relation to the properties of the particles we are interested in. This will explain why the trigger will help the detection of D^* mesons and eventually B mesons. Then we will analyse the results of the implementation of the trigger in Pythia. The trigger particles are discussed, their properties and distributions are analysed and after that, we make some remarks on the triggering process before starting with the results of the trigger bias. The analysis of the functioning of the trigger in this chapter will help us to understand better the results of the following chapters.

5.1 Theoretical background

As already explained in chapter 3: the EMCal detector works by measuring charged particles which then, in a particular detector cell, deposit all their original energy. This energy is measured by the detector. When the trigger mechanism is activated, the full ALICE detector will only turn on to record a collision event when the EMCal has given a signal that a charged particle above a specified energy threshold has been detected. The energy threshold is currently set at 5 GeV. This value will therefore be the main study case for this thesis, but the alternative of 2 GeV will also be discussed, as this was the trigger threshold used in the 8 TeV proton-proton collision data taking in 2012.

5.1.1 Functioning of trigger

Our motivation for triggering on the detection of collision events is that it will enhance the D^* meson yield, that it will shift the transverse momentum

distribution of the mesons and that it will increase the ratio of the beauty originated mesons. To understand this, we have to study the relation of the D^* with the trigger particles.

The trigger particles mainly consist of electrons and photons, which are common final-state particles in a collision. However, the high energy threshold for the EMCAL trigger will cause only specific electrons and photons to produce a trigger signal. The idea is that trigger particles will mainly have their origin in heavy-flavour quarks and related hadrons. Those heavy-flavour quarks, charm and beauty, have a much higher rest mass than other quarks. Therefore, they have more energy to eventually produce particles with a high velocity and therefore high momentum. We expect that particles which reach the energy threshold will mainly come from heavy-flavour quarks. Further on we will call these particles, originating in charm or beauty quarks, heavy-flavour (HF) particles.

The energy threshold for the trigger particles will not only result in an increase in the presence of HF quarks and mesons in the registered events, but will also increase the mean momentum of the HF quarks and mesons themselves. This is because a selection of high momentum trigger particles means a selection on the available energy in its decay chain and therefore also a bias for D^* mesons with higher momentum. This is an indirect selection and will not mean a hard cut on the momentum of D^* mesons - as it is on the momentum of the trigger particles - but it will increase the mean momentum of detected mesons. This bias will be analysed in chapter 6.

Moreover, the value of the energy threshold will influence the fraction of the presence of beauty to charm particles. Beauty quarks are 3 to 4 times heavier than charm quarks¹. This means that beauty particles have more energy to put in kinetic energy. The momentum distribution of beauty induced electrons will be shifted to higher values compared to charm induced electrons. This will cause the trigger to be biased for triggering on beauty. This bias will be studied in chapter 7.

This line of reasoning already gives us a strong reason for using a trigger to enhance the presence of HF particles. The assumption in this argument which yet has to be argued for is that HF quarks produce electrons and photons at all. In order to learn this, we study the fragmentation fractions of HF quarks and branching fractions of HF hadrons.

5.1.2 Fragmentation and branching fractions

In this section, we analyze if electrons can come from decays of HF hadrons. From the fragmentation fractions of the c and b quark we learn that the quarks mainly hadronize into mesons, notably any D meson for charm and B meson for beauty. The fragmentation fraction $c \rightarrow D^0$ is about 54%, the

¹ 4.18 ± 0.03 compared to 1.275 ± 0.025 GeV/ c^2 [20].

fraction $c \rightarrow D^+$ about 22% [23], including their charge conjugates as with every decay from now on. All other produced D mesons eventually decay into one of these two. Now we consider the branching fractions of these two mesons. We go through the inclusive decay modes where the D meson decays in anything + an electron (or positron). For the D^0 the branching fraction is 6.5% [22], for the D^+ 16.1% [21]. Also accounting for the decay fractions of the heavier D mesons, we have the average of 8% for the inclusive mode $c \rightarrow D \rightarrow e^-$. This means that 8% of all charm quarks result in an electron, the same for both their antiparticles (anti-charm and positron).

For the b quark and B mesons we can calculate the branching fraction of the inclusive mode $b \rightarrow B \rightarrow e^-$ in the same way and we get a fraction of 11% [24].

For photons it is more difficult to determine the branching fractions. Photons can be produced in several different ways; they have no separate conservation law and are often a side product of decays and interactions. It is difficult to say how much photons a HF quarks will produce. A lot of final particles decay into photons and in many decays a photon is also emitted, but not added to the decay mode in the books. We can safely say that HF quarks eventually produce a lot of photons, but we cannot say how many. We have to determine experimentally the effects of triggering on energetic photons, we will not theorize about it in this thesis.

From all these branching fractions we conclude that HF quarks can produce electrons and photons. For electrons we expect about 10% of the quarks to produce an electron. For photons this is unsure. Photons however are produced in a lot of ways, of which many result in highly energetic photons. Therefore, we expect energetic photons to be a less strong indication of HF quarks than energetic electrons.

5.1.3 Trigger types

In the real ALICE detector, the EMCal itself cannot distinguish between electrons and photons. It is currently possible to identify the particles captured in the EMCal, by tracing them back in other detectors, but this analysis is done after the collisions are recorded. In ALICE, an EMCal trigger would therefore be triggering on both photons and electrons. The EMCal trigger will have a combined bias of a photon trigger and electron trigger. After the collisions are recorded, data analysis can distinguish between electron and photon triggered collision recordings, in order to create subsamples of electron and photon triggered events. In this thesis, we compare those different trigger samples to determine the best option for the detection of D^* mesons.

Luckily, in Pythia we are able to study all properties of the produced particles, including the type of particle and its origin. This gives us the opportunity to analyse the specific effects of many different types of triggers

and to combine them. We analyse both very specific ones, to check our theoretical expectations, and very general ones, to simulate the effect of a realistic EMCal trigger. In this study, we analyse the effect of the following 10 triggers, where all of the trigger particles have the condition of being in the physical range of the EMCal, as mentioned in chapter 3 and 4. Also, the particles must have an energy above 5 or 2 GeV. These two thresholds double the amount of triggers to 20. As said before, the antiparticles of all mentioned particles are also included.

- Electrons from the decay chain of a charm quark (c electrons)
- Electrons from the decay chain of a beauty quark (b electrons)
- Electrons from the decay chain of a charm or beauty quark (HF electrons)
- All electrons
- Photons from the decay chain of a charm quark (c photons)
- Photons from the decay chain of a beauty quark (b photons)
- Photons from the decay chain of a charm or beauty quark (HF photons)
- All photons
- Kaons, as a case of a hadron trigger
- All photons and electrons, the combined trigger

The kaon trigger was included, in order to obtain a basic understanding of the effect a kaon trigger would have on the D^* yield. The discussion of the kaon trigger is placed in Appendix A. In the next sections, I will discuss the results of the trigger implementation in Pythia.

5.2 Electron trigger

In this section, we investigate the electrons which were simulated in the collisions in Pythia. As said in chapter 4, we have two different settings for the simulation: HF forced and minimum bias. We will discuss them both here, as they each reveal us information about the triggering process. Later on we will make the choice for minimum bias, as I already mentioned in chapter 4. In figure 5.1 we see the transverse momentum distribution for all electrons for both HF forced and minimum bias, in the second plot the HF forced over minimum bias ratio of the two distributions. We understand from the plots that the amount of high-momentum electrons for the forced

setting is higher. We can explain this by the enhanced presence of HF quarks caused by that setting, which are the main cause of energetic electrons.

The red lines in the figure 5.1 give both threshold values for the trigger, notably 5 and 2 GeV. In this high momentum limit $E \gg m_0 c^2$ the energy threshold of 5 GeV gives a momentum value of about 5 GeV/c, so we can also use the p_T distribution instead of the E distribution. We see that most electrons are below the threshold. The ratio of electrons which fulfill the threshold over all electrons is given in table 5.1. The ratio is extremely low in general. For the minimum bias setting, the ratio is about 3 times lower than for the forced setting. Because the ratio of all electrons in HF forced over minimum bias is a factor of 2, in the HF forced setting there is a strong enhancement of high momentum electrons and a suppression of low momentum electrons compared to the minimum bias sample. We can also observe that in the right panel of figure 5.1, where the ratio HF forced of minimum bias is plotted. There we measure a strong enhancement in the forced sample of electrons with energies between 1 and 15 GeV, compared to the minimum bias sample.

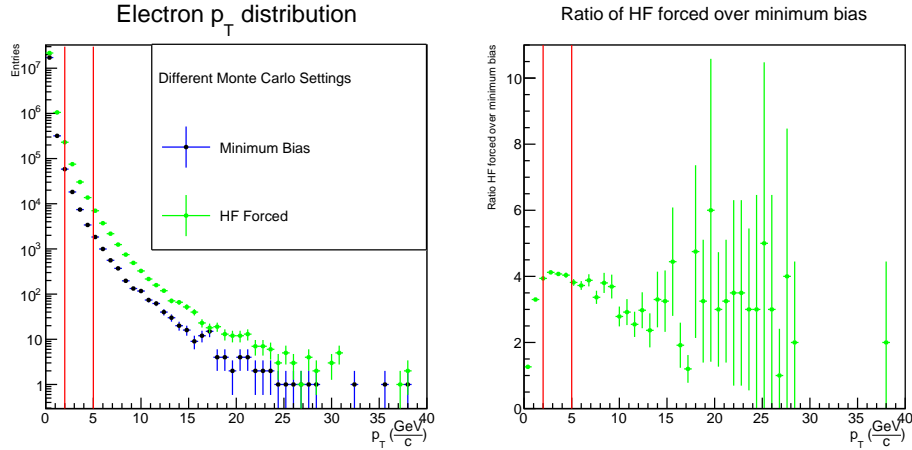


Figure 5.1: Transverse momentum distribution (p_T) for all electrons for both HF forced and minimum bias Pythia settings. Left panel: distributions of both settings. Right panel: ratio of HF forced over minimum bias distributions. The red lines represent the 5 and 2 GeV energy thresholds.

Trigger energy threshold	HF forced	Minimum bias
5 GeV	13.10 ± 0.05	4.54 ± 0.04
2 GeV	158.1 ± 0.2	52.2 ± 0.5

Table 5.1: Amount of electrons which fulfill the trigger threshold per 10,000 electrons.

The next step is to determine the amount of trigger events those electrons

will produce. A trigger event is an event which has a minimum of 1 particle which meets the trigger criteria. As said in chapter 3 and 4, besides the energy threshold, the trigger criteria also include the physical ranges of the EMCal detector. In table 5.2 the amount of trigger events per 10,000 events is given.

The trigger will select only a few events per 10,000 collisions. The amount of events ALICE will record per second in the EMCal trigger mode, will therefore be much lower than its maximum. This will cause ALICE in the same time period to produce less events than in minimum bias mode. However, the expectation is that triggering will make up for less events by selecting more *interesting* events. We present the results for that increase in event quality in the next chapter.

Trigger energy threshold	HF forced	Minimum bias
5 GeV	0.61 ± 0.01	0.172 ± 0.003
2 GeV	7.23 ± 0.04	1.84 ± 0.03

Table 5.2: Amount of electron trigger events per 10,000 events.

Now we will analyze the distribution of the different types of electrons with respect to their origin: heavy-flavour (HF) electrons, beauty (b) electrons or charm (c) electrons. This b or c origin means if the electron is produced in the decay chain of a particle, which was formed by fragmentation of a b or c quark. HF means if the electron comes from either a b or c quark. In figure 5.2, the ratio of those types of electrons over all electrons is depicted, for the two Pythia settings.

For energetic electrons in the HF forced setting, the ratio HF electrons over all electrons is close to 1: nearly all energetic electrons are HF electrons. In the low p_T region, up to 2 GeV/c, the c electrons dominate. Above 5 GeV/c, the ratio stabilises at 80% b electrons and 20% c electrons.

In the minimum bias setting, there are much more ‘background’ electrons, which do not come from HF quarks. Those will contaminate the working of the trigger, as they will produce trigger events without a correlation with D^* mesons. This gets better for higher p_T , but the HF ratio in minimum bias remains lower than in the forced sample. Still, especially for the electron, the beauty ratio is high for high p_T . This is interesting, because it means the 5 GeV trigger threshold will boost the ratio of beauty compared to charm induced electrons. This will definitely cause the trigger to have an effect on the beauty over charm ratio for the D^* origin. We investigate this trigger bias in chapter 7.

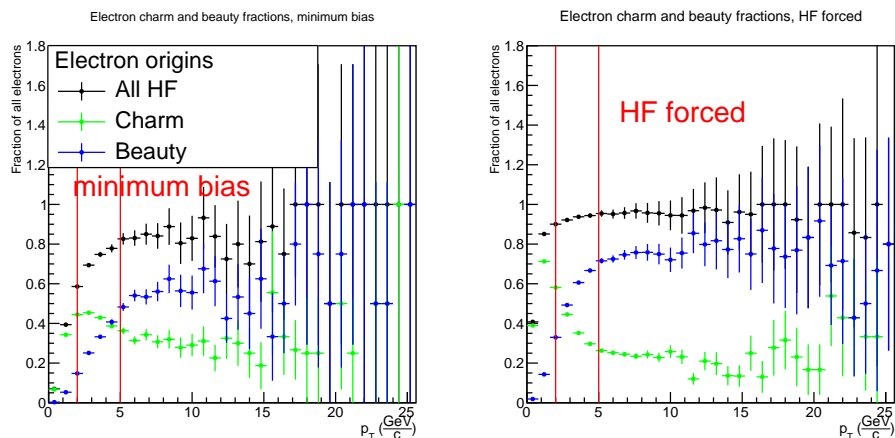


Figure 5.2: Ratio of the transverse momentum (p_T) distribution of HF, c or b electrons over all electrons. Left panel: for the minimum bias sample. Right panel: for the HF forced sample. The red lines represent the 5 and 2 GeV energy thresholds.

5.3 Photon trigger

We can make the same analysis for photons. In figure 5.3, the transverse momentum distribution for all photons is illustrated, for both settings. The red lines again give the trigger thresholds. Because photons are massless particles the following equation holds: $E = pc$. The transverse momentum threshold will precisely be 2 or 5 GeV/c. From the plot we see that the minimum bias setting actually has more energetic photons. In the right hand panel, we observe the ratio of the HF forced distribution over the minimum bias distribution to be below 1. As it seems, the presence of forced HF quarks actually suppresses energetic photons. Apparently, more of the available energy is used for producing photons in minimum bias events and in HF forced events more energy is used for other particles.

The ratio of photons, which make the threshold over all photons is given in table 5.3. For 5 GeV the ratio is very low, although in the minimum bias setting it is higher than in the forced setting. For 2 GeV it is much higher, so this will boost the amount of 2 GeV photon trigger events. In table 5.4 the amount of photon trigger events per 10,000 events is given. Because of more energetic photons being present, minimum bias produces more photon trigger events. For 2 GeV, the amount of events increases drastically.

We can inspect the origin of the photons, as we did for the electrons. In figure 5.4, the ratio of HF, c or b photons over all photons is depicted, for both the HF forced and minimum bias settings. Although nearly all energetic electrons were HF electrons, this is quite different in the case of photons. For the forced setting only a maximum of 50% of all photons are HF photons

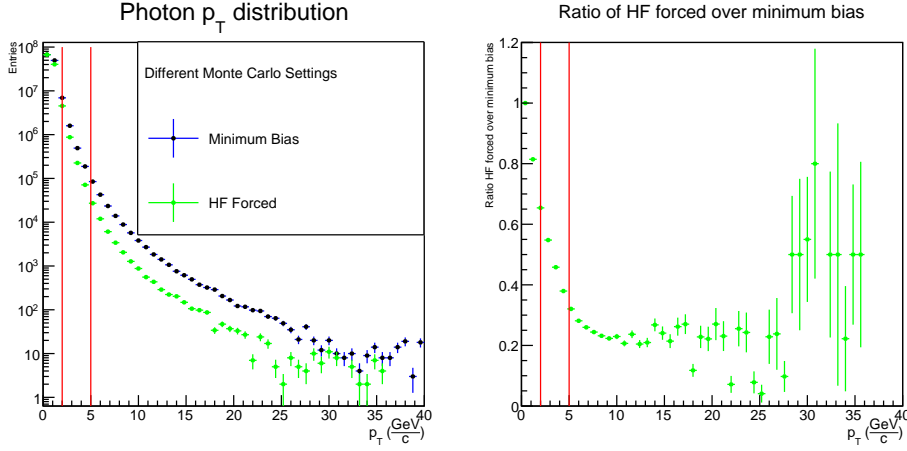


Figure 5.3: Transverse momentum (p_T) distribution for all photons for both HF forced and minimum bias Pythia settings. Left panel: distributions of both settings. Right panel: ratio of HF forced over minimum bias distributions. The red lines represent the 5 and 2 GeV energy thresholds.

Trigger energy threshold	HF forced	Minimum bias
5 GeV	11.2 ± 0.3	30.1 ± 0.6
2 GeV	508 ± 3	745 ± 4

Table 5.3: Amount of photons which make the trigger threshold per 10,000 photons.

and most of those HF photons are from charm. For minimum bias this is even worse: only 10% of the photons are from HF quarks. This means that an EMCAL photon trigger will be dominated by non-HF photons. Although we have expected this from the weak relation of photons with the D^* meson, this is unfortunate, as those non-HF photons will not have a correlation with D^* mesons as strong as HF photons have. A photon trigger will therefore not cause a strong bias on the D^* meson yield. We will see the results of the photon trigger bias in chapter 6.

Another result from figure 5.4 is the low beauty fraction, in both HF forced and minimum bias. Because of this, the photon trigger will probably not cause a beauty enhancement, unlike the electron trigger. The effect of the electron, photon and combined triggers on the beauty fraction will be studied in chapter 7.

Trigger energy threshold	HF forced	Minimum bias
5 GeV	2.0 ± 0.4	6.1 ± 0.6
2 GeV	77 ± 3	154 ± 4

Table 5.4: Amount of photon trigger events per 10,000 events.

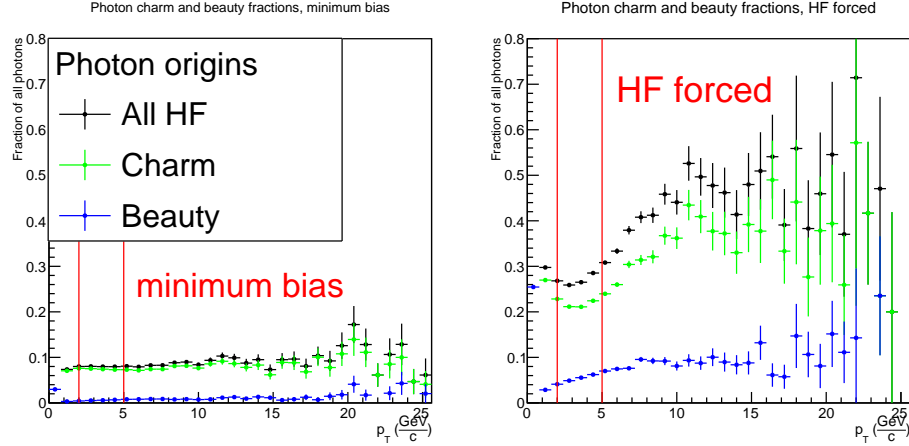


Figure 5.4: Ratio of the transverse momentum distribution of HF, c or b photons over all photons. Left panel: for the minimum bias sample. Right panel: for the HF forced sample. The red lines represent the 5 and 2 GeV energy thresholds.

5.4 Combined trigger

Although the EMCal can, in combination with tracking detectors, distinguish photons from electrons, this analysis is done after the collisions are recorded. Therefore, we have to consider a trigger which combines the input of photons and electrons, to find out what the resulting bias on the D^* production would be. When we compare the tables 5.2 and 5.4 we must first conclude that the presence of photons dominates the presence of electrons in the minimum bias setting. This holds especially for the 2 GeV, and to a lesser extent for the 5 GeV threshold. A combined trigger in the minimum bias setting would therefore closely match the results of a pure photon trigger. Because the minimum bias configuration most closely represents real LHC collisions, this means for the ALICE detector that implementation of the combined trigger will, for most distributions, mean the implementation of a pure photon trigger. In this thesis, the electron, photon and combined trigger bias, for both the 5 and 2 GeV threshold, will all be discussed separately.

5.5 Different Pythia configurations

In chapter 4 I discussed the two Pythia settings (HF forced and minimum bias). As we concluded from the figures in this chapter, the electron and photon distributions are different for the two settings. The forced configuration gives a cleaner sample of HF electrons and photons, the minimum bias sample is contaminated with a lot of non-HF electrons and photons, still passing the trigger threshold. Originally, I used the HF forced setting, mainly for the practical reason that HF forced results in more HF quarks and therefore more interesting events for my thesis. I already explained in chapter 4 why I switched to the minimum bias setting: the HF forced configuration turned out to have a bias on the enhancement distributions, not being in agreement with the realistic minimum bias configuration. Now with the results of this chapter we can understand that bias better. The contribution of non-HF trigger particles in the minimum bias sample is not present in the HF forced sample, in which nearly all trigger particles come from a HF decay. For example, we see that most energetic photons in the minimum bias sample do *not* come from HF decays, contrary to the photons in the HF forced sample. Those non-HF trigger particles have no correlation with the presence of D^* . Because of that, this contribution has strong effects on the distributions of the triggered D^* in the realistic minimum bias sample. While it gives less statistic in the same number of events, minimum bias gives realistic results which are more like what we will find when using an EMCal trigger in ALICE. It is therefore better to use the minimum bias sample, which I will do from now on.

Chapter 6

Trigger bias on D* yield

In this chapter, we discuss the results of the implementation of the trigger for the production of D* mesons. We compare the D* yield in minimum bias and triggered events, as a function of both p_T , ϕ and η . The goal is to find the enhancement factor for the presence of the mesons as a result of the implementation of a specific trigger. The enhancement factor determines how much more mesons are produced or detected in the same number of events as compared to normal, in this case non-triggered, events. We can calculate the enhancement factor as a function of transverse momentum (p_T), pseudorapidity (η) or of the polar angle in the transverse plane (ϕ). The enhancement factor is calculated with formula 6.1. Here, N is the number of events, $f(x)$ is the distribution for a certain variable x (i.e. p_T , η or ϕ).

$$Enhancement\ factor = \frac{N_{minimum\ bias}}{N_{trigger}} \frac{f_{trigger}(x)}{f_{minimum\ bias}(x)}. \quad (6.1)$$

All D* mesons in the following sections are ‘detected’ in the physical range of the ALICE detector: $|\eta| < 0.9$ and all ϕ , as mentioned in chapter 3.

6.1 Minimum bias D*

The term ‘minimum bias’ has already been used in this thesis, pointing to the most realistic Pythia configuration, contrary to the HF forced configuration. However, I already mentioned that only the minimum bias sample is used in the rest of this thesis. From now on ‘minimum bias’ will mean *no trigger used*.

The D* meson can decay in many different ways. These ways are called decay *channels*. In the ALICE data analysis, D* mesons are reconstructed by tracing the following possible decay products: two pions and a kaon. D* which do not decay into these products will not be found. We therefore have to check if the D* mesons which decay through those specific decay channels

are not in any way different than the rest of the D^* . In figure 6.1, the p_T distribution of all¹ D^* mesons are illustrated, together with the distributions of the D^* which decayed through a specific decay channel. The first decay channel² is $D^{*+} \rightarrow D^0 + \pi^+$ and the second constitutes two consecutive decay channels: $D^{*+} \rightarrow D^0 + \pi^+$ and $D^0 \rightarrow K^- + \pi^+$. In the panel, the first branching ratio is in agreement with the values in the literature, the second is off by a few percent³. This is probably caused by a wrong analysis of the decay channel in the simulation code, but the error won't matter for this thesis as I will explain.

The shape of the p_T distribution is the same for all three. This is also shown in the right plot, where the ratio of the D^* with the decay channels over all D^* is shown. The ratio is constant, which means that the distributions have the same shape. This was also checked for the ϕ and η distributions and they yield the same result. This means that any differences between all D^* , and the D^* that can eventually be measured, can be ignored. For the practical reason to have more statistics, I therefore chose to include the D^* with all decay modes in the rest of the thesis. We have to keep in mind however that only a fraction of these D^* mesons can be recovered by current data analysis.

This line of reasoning has not accounted for the effect on the triggering process the different D^* decay channels may have. A D^* can decay into an electron, instead of decaying through the observable decay channels which were mentioned. This electron can then cause the trigger to give a signal. Although the trigger electron in this case does produce a trigger event in which a D^* meson is present — which is the ultimate goal of using a trigger — this D^* cannot be measured exactly *because* it decayed into an electron, which represents a currently non-observable decay channel. A significant part of all trigger signals will thus yield events with D^* mesons which are non-observable. This is unfortunate, although maybe in the future we can detect the D^* mesons, which decayed through other channels, as well. In this thesis, this effect is ignored, as we include all D^* in the analysis. In the outlook in the last chapter I will present some possible ways for future studies to investigate the influence of these D^* , decaying into electrons, on the trigger bias.

¹In the $|\eta| < 0.9$ region, as it will always be from now on.

²Also including all their charge-conjugates.

³68% for the first [25] and 3.9% for the second decay channel [22].

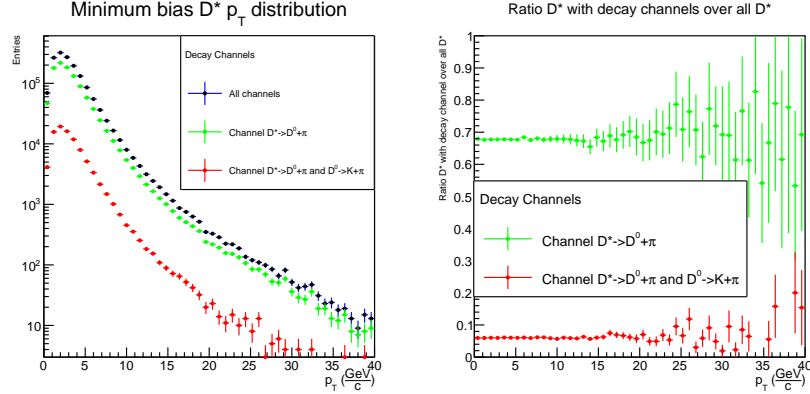


Figure 6.1: Left panel: transverse momentum distribution of D^* mesons in minimum bias, for different decay modes. Right panel: ratio of the distribution of D^* mesons with specified decay channel and all D^* mesons.

6.2 Overall enhancement

In table 6.1 the overall enhancement factor is indicated for the different triggers. This overall enhancement factor is calculated by replacing in equation 6.1 the distributions $f(x)$ by the integration of the D^* distributions (trigger and minimum bias) over the whole range of ϕ .

We see a big difference in the enhancement caused by the electron trigger and the photon trigger. We can explain this by referring to the discussion of the different triggers in chapter 5, where we observed that photons primarily come from sources other than HF particles (see figure 5.4). This results in a weak correlation between energetic photons and D^* mesons, as opposed to the strong correlation between energetic electrons and D^* mesons. For the combined trigger, we can conclude that its bias is dominated by the bias of the photon trigger. In the next chapters, we will further explore the enhancement factor as a function of ϕ , η and p_T , for all different trigger samples.

Event sample	Overall enhancement factor
5 GeV electron trigger	41 ± 1.3
5 GeV photon trigger	5.94 ± 0.08
5 GeV electron and photon trigger	6.90 ± 0.09
2 GeV electron trigger	30.5 ± 0.3
2 GeV photon trigger	4.67 ± 0.01
2 GeV electron and photon trigger	4.93 ± 0.02

Table 6.1: Overall enhancement factor for the D^* meson yield in different trigger samples, for D^* in $|\eta| < 0.9$.

6.3 Trigger bias for ϕ and η distributions

Although we are ultimately interested in the p_T distributions, because of the trigger induced shift in the mean p_T and the enhancement for different values of p_T , we will first investigate the ϕ and η distributions. These can tell us in which physical region the D^* mesons are enhanced. Will they be enhanced in the trigger region - in the range of the EMCAL: $|\eta| < 0.7$ and $0^\circ < \phi < 110^\circ$ - or exactly on the opposite side? This will make clear if the triggering electrons and photons have been produced mainly alongside the D^* mesons (in this case the electrons and photons come from the same c or b quark as the D^*) or back-to-back (in this case the electrons and photons come from the antiparticle of the D^* producing quark). It also will give a first impression of the amount of D^* in events, triggered by non-HF particles. We expect non-HF trigger particles to have no correlation with the D^* mesons. The D^* , present in the events those non-HF trigger particles produce, are produced with the same probability as in a minimum bias sample. This will cause the D^* in those events to be randomly distributed over all ϕ and η . We can therefore study the D^* distribution in the ϕ and η regions outside the range (and opposite side) of the EMCAL, in order to have an idea of the amount of trigger uncorrelated D^* in the trigger sample.

5 GeV triggers

In figure 6.2, the enhancement factor is shown as a function of ϕ , for three different trigger samples: the electron, photon and combined trigger with the energy threshold of 5 GeV. The space between the red lines gives the range of the EMCAL: $110^\circ > \phi > 0^\circ$. We clearly observe a strong enhancement in the EMCAL range, most visible for the electron trigger sample, but also present in the other trigger samples. Table 6.2 gives the enhancement factors inside and outside the EMCAL region. In figure 6.3, the enhancement factor is shown as a function of η , for the same three 5 GeV trigger samples. The space between the red lines gives the range of the EMCAL: $|\eta| < 0.7$. Also here, we observe a strong enhancement in the EMCAL range. Table 6.3 gives the enhancement factors inside and outside the EMCAL region.

2 GeV Triggers

In figure 6.4, the ϕ dependent enhancement is illustrated, for the three 2 GeV trigger samples. Table 6.2 gives the enhancement factors inside and outside the EMCAL region. In figure 6.5, the η -dependent enhancement is illustrated. Table 6.3 gives the enhancement factors inside and outside the EMCAL region. In both figures, the 2 GeV trigger samples seem to exhibit the same ϕ and η dependent enhancement as the 5 GeV trigger sample. However, the average enhancement factor is much less for all 2 GeV triggers.

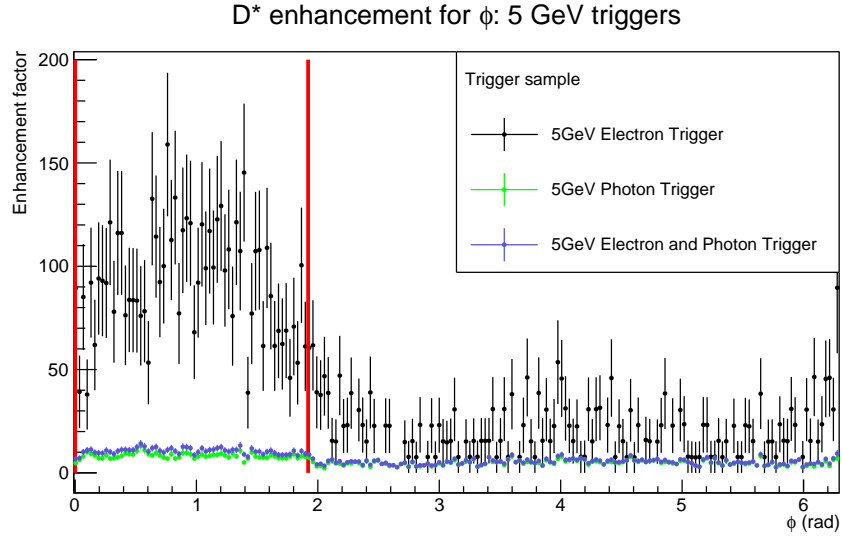


Figure 6.2: D^* meson enhancement for different 5 GeV trigger samples, in $|\eta| < 0.9$, as a function of the polar angle in the transverse plane (ϕ). The region between the red lines is the EMCAL region: $110^\circ > \phi > 0^\circ$.

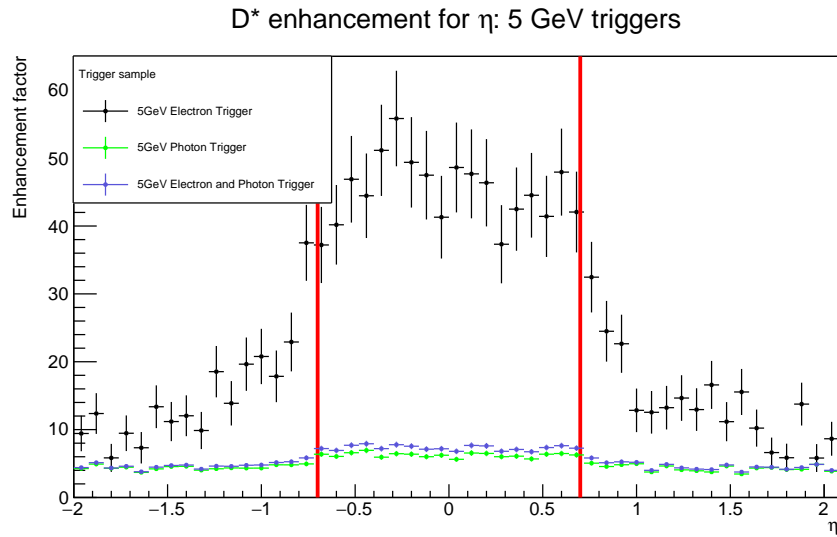


Figure 6.3: D^* meson enhancement for different 5 GeV trigger samples, in all ϕ , as a function of pseudorapidity (η). The region between the red lines is the EMCAL region: $|\eta| < 0.7$.

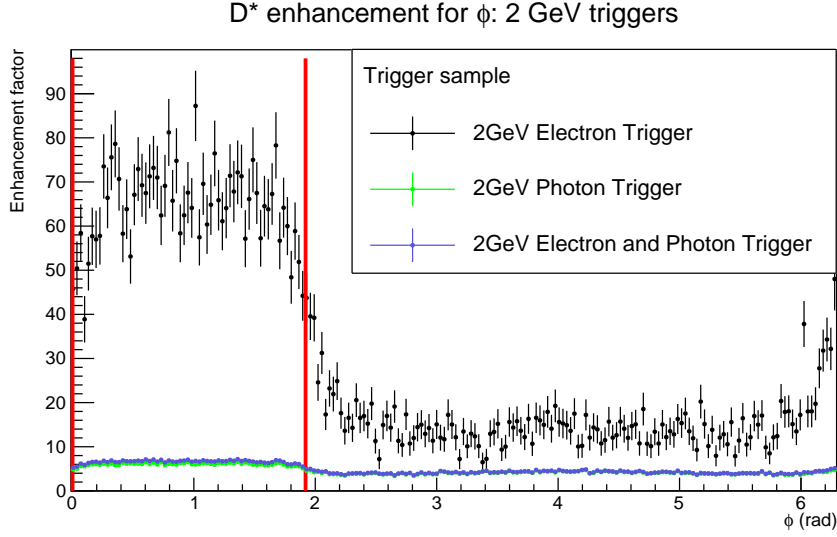


Figure 6.4: D^* meson enhancement for different 2 GeV trigger samples, in $|\eta| < 0.9$, as a function of the polar angle in the transverse plane (ϕ). The region between the red lines is the EMCAL region: $110^\circ > \phi > 0^\circ$.

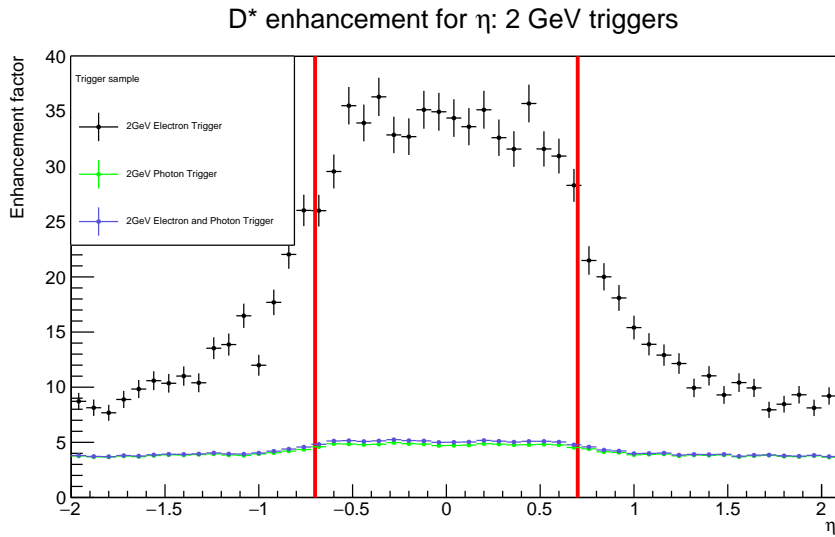


Figure 6.5: D^* meson enhancement for different 2 GeV trigger samples, in all ϕ , as a function of pseudorapidity (η). The region between the red lines is the EMCAL region: $|\eta| < 0.7$.

Conclusion for the trigger bias for ϕ and η distributions

In ϕ and η there are two different regions for the enhancement of the D^* yield: inside the EMCAL range and outside the range. We fit the enhancement factor in those regions with a straight line and find the two average enhancement factors for every trigger. The results for the ϕ distributions are listed in table 6.2 and those for the η distributions in table 6.3.

In trigger events, D^* mesons are systematically more observed in the $110^\circ > \phi > 0^\circ$ and $|\eta| < 0.7$ regions than outside those regions. Hence, the mesons are more often detected in the same region as the trigger particles. This means that the trigger electrons and photons on average are directed alongside the path of the mesons. This leads to the conclusion that both the trigger particles and the mesons most often have their origin in the same decay chain. It could be that some triggering electrons and photons come from the decay of the produced D^* mesons.⁴ It is also possible that the electrons and photons have their origin earlier in the decay chain; they are produced before, or simultaneous with, the D^* meson. What we can conclude from this, is that the D^* meson and the triggering particle most often stem from the same HF quark, instead of the other quark of the quark-antiquark pair.

In the region outside the EMCAL, we still see some enhancement. This enhancement is due to the contribution of events triggered by particles, which are uncorrelated with the mesons: non-HF electrons and photons. The D^* mesons in those events are randomly distributed over all ϕ and η . Even in this region, the mesons are more present in the trigger sample than in the minimum bias sample, as indicated by the enhancement factor greater than 1. Apparently, non-HF trigger particles still cause a trigger bias for D^* yield. For electrons, this bias is stronger than for photons, as the enhancement factor outside the EMCAL region is much higher for electrons.

Event sample	Inside EMCAL region	Outside EMCAL region
5 GeV electron trigger	83 ± 3	15.5 ± 1
5 GeV photon trigger	8.1 ± 0.2	4.53 ± 0.09
5 GeV electron and photon trigger	10.4 ± 0.2	4.96 ± 0.09
2 GeV electron trigger	63.0 ± 0.9	13.8 ± 0.3
2 GeV photon trigger	6.01 ± 0.03	4.06 ± 0.02
2 GeV electron and photon trigger	6.59 ± 0.03	4.17 ± 0.02

Table 6.2: D^* meson enhancement factor for different trigger samples, in $|\eta| < 0.9$, in two regions of ϕ : inside and outside the EMCAL acceptance ϕ range, being $110^\circ > \phi > 0^\circ$.

⁴See for the discussion of this effect section 6.1.

Event sample	Inside EMCAL region	Outside EMCAL region
5 GeV electron trigger	45 ± 1.5	11.8 ± 0.5
5 GeV photon trigger	6.2 ± 0.1	4.34 ± 0.05
5 GeV electron and photon trigger	7.3 ± 0.1	4.60 ± 0.06
2 GeV electron trigger	32.5 ± 0.4	11.3 ± 0.2
2 GeV photon trigger	4.78 ± 0.02	3.87 ± 0.01
2 GeV electron and photon trigger	5.06 ± 0.02	3.95 ± 0.01

Table 6.3: D^* meson enhancement factor for different trigger samples, in all ϕ , in two regions of η : inside and outside the EMCAL acceptance η range, being $|\eta| < 0.7$.

6.4 Trigger bias for p_T distributions

In this section, we investigate the D^* meson enhancement as a function of the transverse momentum p_T of the meson. As I explained in chapter 5, the high energy threshold of the trigger will cause a selection on the available energy in the HF quark decay chain in trigger events. This will increase the mean energy, and mean p_T , of the D^* meson. We expect mesons with lower p_T to be suppressed and mesons with higher p_T to be enhanced by the trigger. We determine after which value of p_T the enhancement factor stabilizes to a constant, and what this constant maximum enhancement will be. This will vary for each trigger.

5 GeV Triggers

In figure 6.6, the p_T distributions are plotted for different 5 GeV trigger samples. The trigger distributions are combined with the minimum bias p_T distribution, after having been normalized to the number of events. We conclude that the mean p_T has shifted under influence of the trigger. The various mean values for the p_T distributions are listed in table 6.4.

In figure 6.8, the p_T dependent enhancement plots are shown for the same 5 GeV triggers. The figure shows the various triggers to exhibit low enhancement at low p_T , rising fast up to a point where the enhancement flattens out to a maximum. The colored line is the maximum enhancement factor at the upper limit of p_T . I made an assumption for the value of p_T where we observe this flatness. The maximum enhancement factor is then obtained by fitting a straight line from this value of p_T . This enhancement factor strongly depends on the subjective value of p_T where we assume flatness. It gives an idea of the maximum enhancement, but it is not meant to be an objective value. The list of these maximum enhancement factors with the minimum p_T value used for the fitting is listed in table 6.5.

2 GeV Triggers

In figure 6.7, the p_T distributions are plotted for different 2 GeV trigger samples. The various mean values for the p_T distributions are again listed in table 6.4. In figure 6.9, the measured enhancement factor is depicted as a function of p_T , for the same trigger samples. The list of the maximum enhancement factors with the p_T minimum value used is listed in table 6.5. The determination of the maximum enhancement was done in the same way as for the 5 GeV triggers. However, the value of p_T where we assume flatness has changed for the 2 GeV trigger samples.

Conclusion for the trigger bias for p_T distributions

The enhancement plots are quite different for the electron trigger samples compared to the photon and combined trigger samples. The electron trigger causes a much stronger enhancement for all values of p_T . We already saw this stronger enhancement in the ϕ and η plots, now we conclude that the electron trigger enhancement is high in both the low and high p_T limit. The value of p_T from where the enhancement flattens out to a maximum is comparable for all triggers with the same energy threshold.

When we compare the two energy threshold, we observe a great difference between the 5 and 2 GeV triggers. All 5 GeV triggers have a maximum enhancement of about 10 times the maximum enhancement of the same 2 GeV trigger. We see that same 5 GeV trigger bias for high p_T mesons reflected in the increased mean p_T value, listed in table 6.4.

In the increase of the high p_T D^* meson yield, the 5 GeV triggers perform much better than the 2 GeV triggers. Between all 5 GeV triggers, the electron trigger stands out, by enhancing the presence of high p_T D^* up to a factor of 1300 compared to the minimum bias sample.

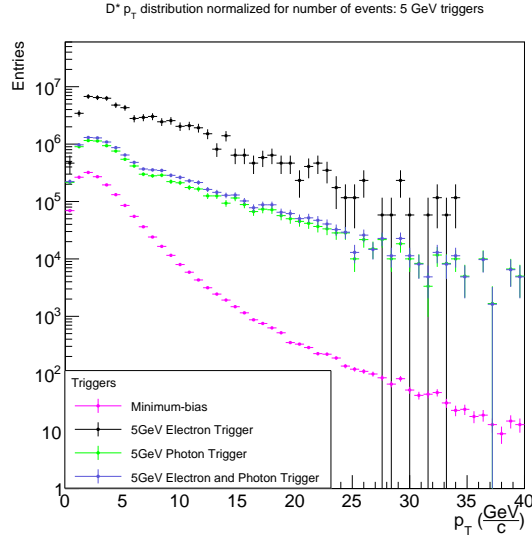


Figure 6.6: D^* meson yield as a function of transverse momentum (p_T) for different 5 GeV trigger samples. The trigger sample distributions are combined with the minimum bias sample distribution, after all distributions have been normalized to the number of events in the sample.

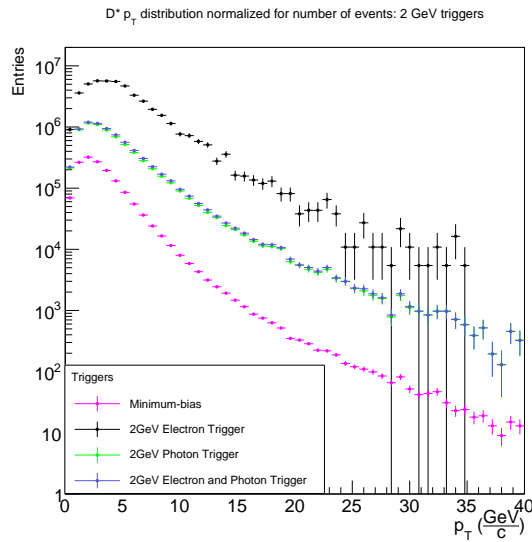


Figure 6.7: D^* meson yield as a function of transverse momentum (p_T) for different 2 GeV trigger samples. The trigger sample distributions are combined with the minimum bias sample distribution, after all distributions have been normalized to the number of events in the sample.

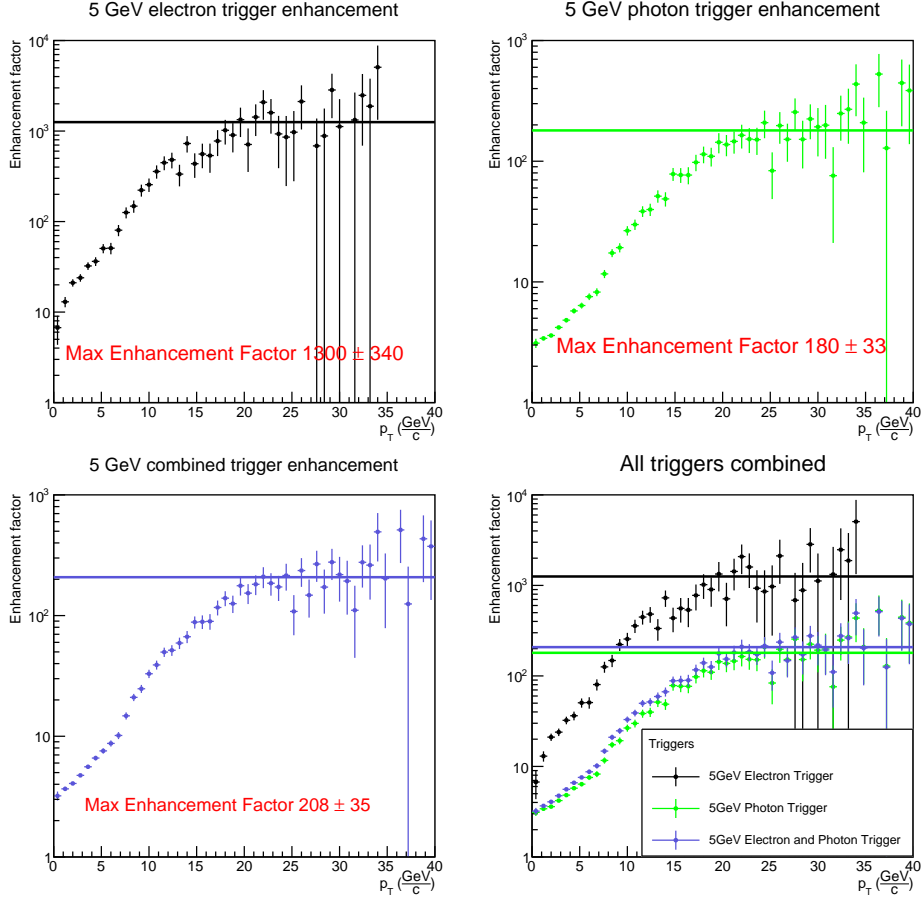


Figure 6.8: D^* meson yield enhancement as a function of transverse momentum (p_T), for different 5 GeV trigger samples. The colored line represents the maximum enhancement factor in the limit of high p_T . These maximum enhancement factors are listed in table 6.5.

Event sample	D^* yield	Mean p_T (GeV/c)
Minimum bias	$1.5146 * 10^6 \pm 1 * 10^3$	3.248 ± 0.002
5 GeV electron trigger	$1.08 * 10^3 \pm 3 * 10^1$	7.3 ± 0.2
5 GeV photon trigger	$5.39 * 10^3 \pm 7 * 10^1$	6.32 ± 0.08
5 GeV electron and photon trigger	$6.44 * 10^3 \pm 8 * 10^1$	6.46 ± 0.07
2 GeV electron trigger	$8.51 * 10^3 \pm 9 * 10^1$	5.14 ± 0.04
2 GeV photon trigger	$1.081 * 10^5 \pm 3 * 10^2$	4.23 ± 0.01
2 GeV electron and photon trigger	$1.154 * 10^5 \pm 3 * 10^2$	4.27 ± 0.01

Table 6.4: Total D^* meson yield, and mean value of the D^* p_T distribution, for different samples.

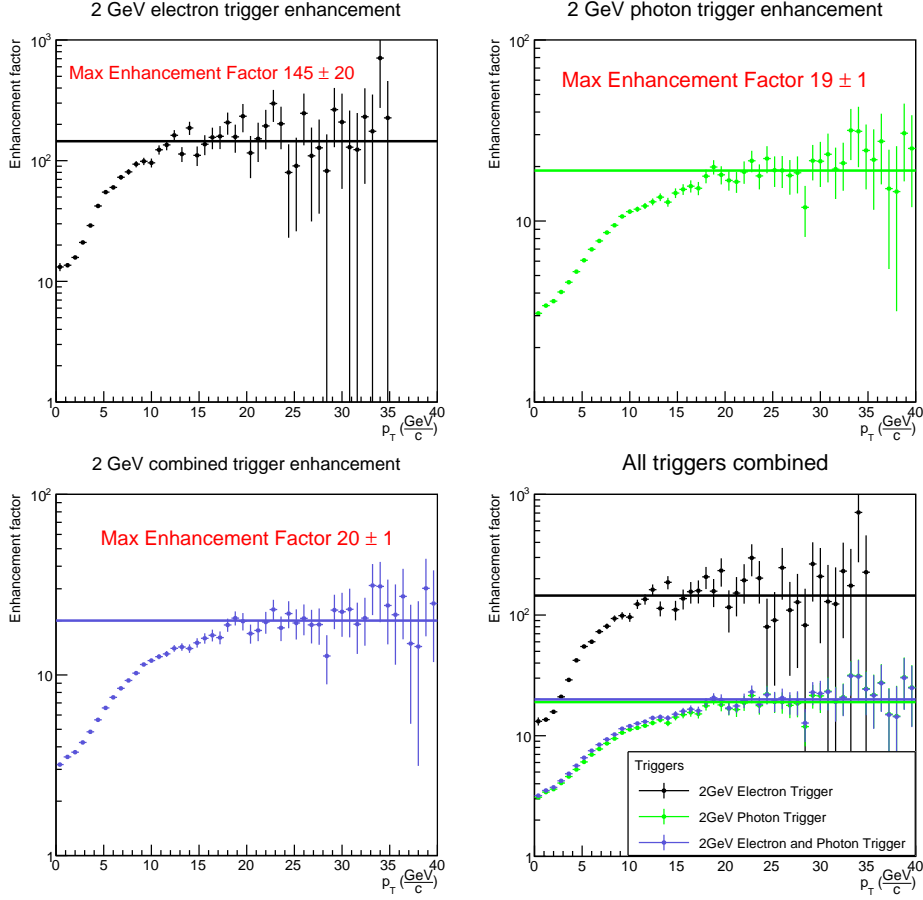


Figure 6.9: D^* meson yield enhancement as a function of transverse momentum (p_T), for different 2 GeV trigger samples. The colored line represents the maximum enhancement factor in the limit of high p_T . These maximum enhancement factors are listed in table 6.5.

Event sample	Maximum enhancement factor	p_{flat} (GeV/c)
5 GeV electron trigger	$1.3 * 10^3 \pm 3 * 10^2$	30
5 GeV photon trigger	$1.8 * 10^2 \pm 3 * 10^1$	30
5 GeV electron and photon trigger	$2.1 * 10^2 \pm 35 * 10^1$	30
2 GeV electron trigger	$1.5 * 10^2 \pm 2 * 10^1$	20
2 GeV photon trigger	$1.9 * 10^1 \pm 1$	25
2 GeV electron and photon trigger	$2.0 * 10^1 \pm 1$	25

Table 6.5: D^* meson maximum enhancement factor for different trigger samples in the limit of high p_T . The p_T value above which the enhancement is assumed to be flat is given as p_{flat} .

Chapter 7

Trigger bias on the beauty fraction

We are interested in D^* mesons, because their origin lies in the fragmentation of HF quarks. One possible origin of the D^* is that a c quark fragmented into a D^* (called prompt D^*). That c quark, before hadronization, possibly interacted with the QGP. Another possible origin is that the D^* meson decayed from a B meson, which consists of a b quark. That b quark also possibly interacted with the QGP.

Beauty quarks are more valuable for the exploration of the QGP than charm quarks, as explained in chapter 3. In the collisions, we therefore want to observe as much b quarks, and products of b quarks, as possible. Those b quark products include a B meson or a D^* meson, coming from a B decay. This D^* is then called a feed-down D^* . In this thesis we call those D^* coming from a beauty decay *beauty* D^* , as opposed to *charm* D^* . This terminology has nothing to do with the content of the meson, as a D^* always consists of an (anti)charm and an (anti)down, but refers to the origin of the D^* .

In Pythia, we studied the origin of all D^* , thereby determining the beauty fraction of all D^* mesons. In this chapter, we analyze the trigger bias on the beauty fraction, in particular the beauty fraction in the origin of the D^* . Whether a c or b quark origin of the trigger particles affects the D^* and its beauty fraction is also discussed. In the end, we will shortly turn our attention to the B meson to study the trigger bias on the B meson yield.

7.1 Beauty quark fraction

Before we analyze the distribution for the D^* and B mesons, we can examine the distributions of the HF quarks before hadronization. In figure 7.1 we see the ratio of charm quarks over beauty quarks as a function of p_T , for minimum bias and different trigger samples. In the minimum bias sample, we observe that the ratio starts at a factor of 100, then for higher p_T quickly

dropping to a stable factor of 1. This means that for high p_T , there are as much c as b quarks. The electron triggers, with both energie thresholds, change this distribution by enhancing the presence of b quarks relative to c quarks: for $p_t > 5$ GeV/c, the fraction charm over beauty is 0.5, which means that there are about 2 times more b than c quarks. The photon trigger is not enhancing the beauty presence. On the contrary: for the 5 GeV photon trigger, we observe it to enhance the presence of charm quarks relative to beauty quarks. The 2 GeV photon trigger simply conserves the charm to beauty ratio of the minimum bias sample. The combined (photon and electron) trigger seeks the middle ground between these two triggers, although at the 2 GeV threshold, the combined trigger is dominated by photons, as we observed before.

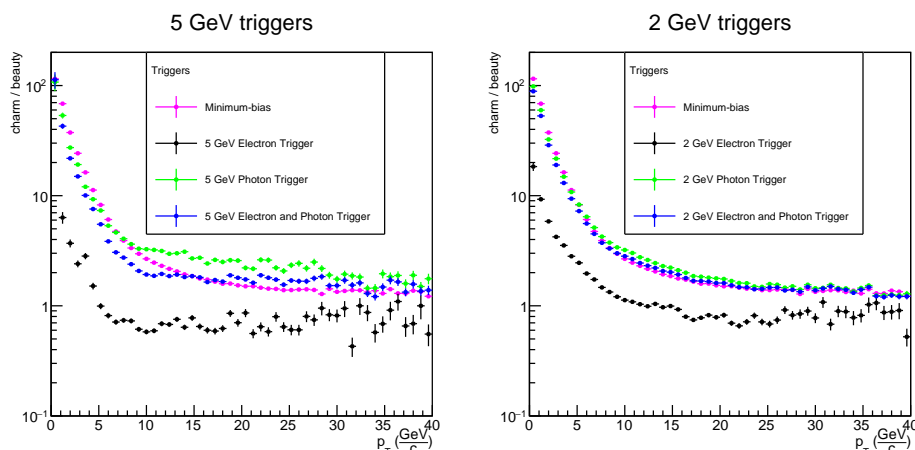


Figure 7.1: Ratio of c quarks over b quarks as a function of p_T , for minimum bias and different trigger samples.

7.2 Trigger origin influence

Just as we can study the c or b origin of the D^* , we can also study the origin of the trigger particles. Not all of them originate in HF decays, but as we saw in figure 5.2 in chapter 5, energetic electrons most often do. We now want to observe the effects of triggering on particles with specific c or b origins, to see if it does enhance the charm or beauty fraction in the D^* mesons, as we expect it to do. According to what we found in section 6.3, the trigger particles most often stem from the same quark as the D^* meson, so there should be a correlation in the origin, being beauty or charm, of the triggering particle and the meson.

Since the beauty fraction in the origin of photons is much lower than in the origin of electrons (figure 5.4), the overall effect of photon triggering on

the beauty fraction will be small. This is reflected in the already discussed figure 7.1. Hence, I will neglect the photon trigger in this section.

In table 7.1, we determine for c originated, b originated and all D^* , which part of the D^* mesons in trigger samples are triggered by b, c or non-HF electrons. We observe that most c and b D^* come from respectively c and b electron triggered events. Still, some percent of the D^* are from events triggered by other electrons. Those electrons have no relation with the mesons, but sometimes cause a trigger signal for an event, which accidentally has a D^* in it. Yet in general, we can say that D^* mesons coming from either a c or b quark, come from events which are triggered most often by respectively a c or b electron.

Another result from the table is the high probability, at the trigger threshold of 5 GeV, of origin neutral D^* to come from b electron triggered events. This means that D^* in general are more often triggered by electrons from b decays than by other electrons at this threshold. We could expect this because of the high b ratio in energetic electrons (figure 5.2 in chapter 5). This result, together with the first result, predicts the enhancement of the beauty fraction in D^* by the 5 GeV electron trigger: because D^* most often are triggered by b electrons (compared to other electrons) and b electrons most often trigger b mesons, the trigger will have a positive bias for D^* coming from b. The results for this bias are presented in the next section.

Trigger electron origin	All D^*	D^* from charm	D^* from beauty
5 GeV electron trigger			
Non-HF	6%	5%	7%
Charm	36%	83%	7%
Beauty	61%	18%	91%
2 GeV electron trigger			
Non-HF	12%	7%	19%
Charm	56%	89%	6%
Beauty	34%	7%	79%

Table 7.1: Percentage of D^* yield from the subsample of events triggered by an electron with specific origin, in the D^* yield from the sample of events triggered by all electrons, for D^* originating from a c or b quark, or all D^* . The percentages do not add up to 100%, because the different trigger samples share many events.

7.3 D^* beauty fraction

In this section, we study the trigger bias on the D^* beauty fraction. The beauty fraction is the ratio of D^* mesons, which come from b quarks (also called B feed down D^*), of all D^* . The average beauty fraction is listed in table

7.2 for all different samples. This fraction is calculated by integration of the ϕ distribution of both D^* , coming from beauty decay, and all D^* , irrespective of their origin. The ratio of these integrals is the beauty fraction. We observe a huge beauty enhancement for the electron triggers, especially the 5 GeV trigger. The beauty fraction is 5 to 6 times higher in the 5 GeV electron trigger sample compared to the minimum bias sample. The photon triggers hardly show a bias for beauty. In the following sections, we explore this beauty enhancement further by studying the beauty fraction as a function of different variables. First, the beauty fraction as a function of ϕ and η is discussed, to see if there is beauty enhancement in certain spatial regions; then the beauty fraction as a function of p_T will be investigated.

To determine the beauty fraction, the beauty D^* distributions are divided by the distributions of origin-independent D^* . The beauty D^* mesons are selected from a different simulation sample than the origin-independent D^* mesons. Therefore, statistical fluctuations can cause some data points for the beauty fraction to have a value greater than 1. This effect could be countered by enlarging the sample size, but for the current samples this effect is visible.

Event sample	Overall beauty fraction
Minimum bias	0.1077 ± 0.0003
5 GeV electron trigger	0.58 ± 0.03
5 GeV photon trigger	0.181 ± 0.006
5 GeV electron and photon trigger	0.245 ± 0.007
2 GeV electron trigger	0.387 ± 0.008
2 GeV photon trigger	0.135 ± 0.001
2 GeV electron and photon trigger	0.151 ± 0.001

Table 7.2: Average fraction of D^* from beauty over all D^* , for different samples. This average fraction is calculated by separate integration of the general and beauty D^* distributions and determining the ratio of those two integrals.

ϕ and η distributions

We want to check if there are certain regions in the detector where beauty is enhanced. This could potentially be useful for separating b from c originated D^* . In figure 7.2, the beauty fraction is plotted as a function of ϕ , for different triggers. We observe no such enhancement. The beauty fraction is constant for all ϕ . In figure 7.3 we plot the same for η . No special enhancement region can be observed. This leads to the conclusion that the b originated D^* mesons are equally distributed over all D^* mesons with respect to space coordinates.

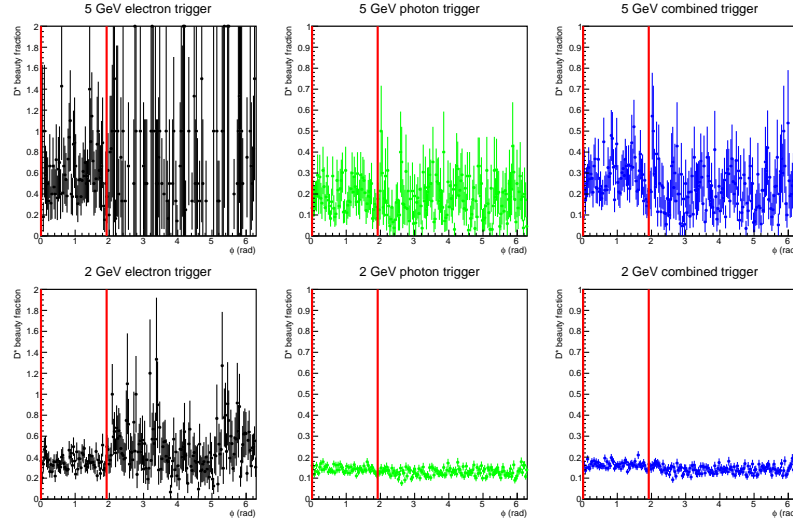


Figure 7.2: Fraction D^* from beauty over all D^* , as a function of ϕ , for different triggers. The red lines give the ϕ range of the EMCAL. In the upper panels: 5 GeV triggers. In the lower panels: 2 GeV triggers. From left to right: electron, photon and combined (electron and photon) triggers.

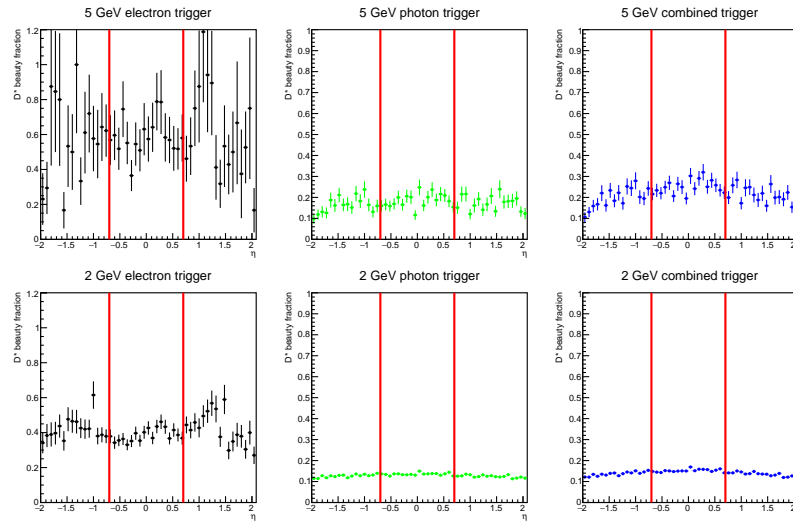


Figure 7.3: Fraction D^* from beauty over all D^* , as a function of η , for different triggers. The red lines give the η range of the EMCAL. In the upper panels: 5 GeV triggers. In the lower panels: 2 GeV triggers. From left to right: electron, photon and combined (electron and photon) triggers.

p_T distributions

We now turn our attention to the beauty fraction as a function of p_T . In figure 7.4 we see the beauty fraction versus p_T in the minimum bias sample. The beauty fraction for low p_T is about 0.1, for higher p_T it grows to 0.2.

In figure 7.5 we see the beauty fraction versus p_T for different trigger samples. Surprisingly, the shapes for the electron trigger samples are quite different from the shape in the minimum bias sample. For the electron trigger, we see a high beauty fraction at low p_T . For higher p_T , the fraction seems to stabilize on the same value as in minimum bias, about 0.2. Apparently, the electron trigger induced beauty enhancement is strong at low p_T and weak at high p_T .

We can understand this if we realize that in the low p_T range, the electrons related to beauty D^* have a higher probability to have enough energy for the trigger threshold, compared to electrons related to charm D^* , as a result of the higher value of available energy in the beauty quark. In the high p_T range however, the energetic charm quark from which a charm D^* with high momentum is an offspring, necessarily also has enough energy to give a high momentum to a produced electron. Charm D^* with high momentum therefore correlate with high momentum electrons, which fulfill the trigger energy threshold with ease. In the high p_T limit, the trigger will not cause an enhancement in the beauty fraction anymore: all HF electrons, beauty and charm originated alike, will have high enough energy in that high p_T limit.

This line of reasoning can only hold when the branching ratio for the inclusive modes $b \rightarrow B \rightarrow e^-$ and $c \rightarrow D \rightarrow e^-$ is about the same. We already found this in section 5.1.2: the branching ratios are 11% and 8% respectively. This small difference is negligible for this discussion.

Contrary to the electron triggers, the photon triggers hardly enhance the beauty fraction. We can explain this by considering the weak correlation between energetic photons and beauty particles, which we found in figure 5.4 in chapter 5.

In table 7.3, the beauty fraction is listed for all samples, for two values of p_T : 1 GeV/c and 10 GeV/c.

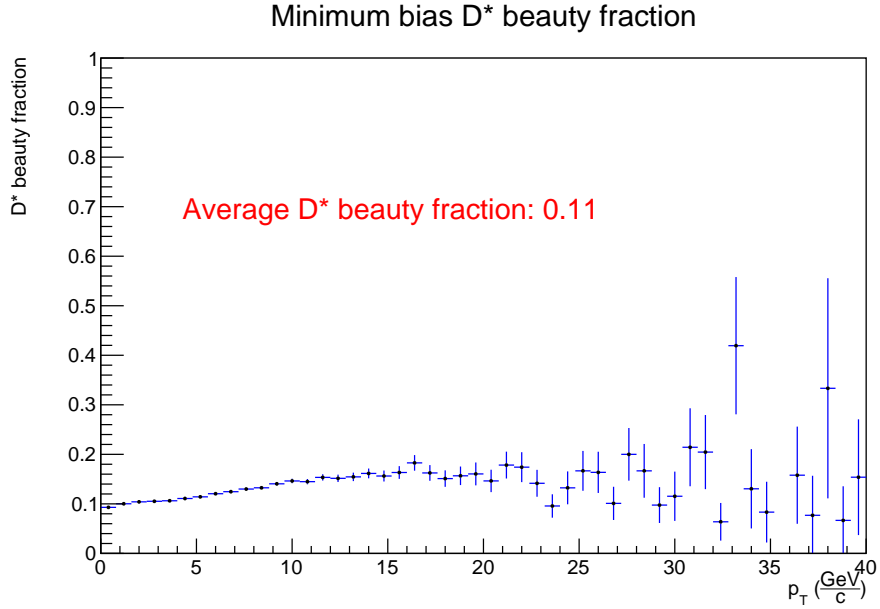


Figure 7.4: Fraction of D* from beauty over all D*, as a function of p_T , minimum bias sample.

Event sample	$p_T = 1 \text{ GeV}/c$	$p_T = 15 \text{ GeV}/c$
Minimum bias	0.100 ± 0.001	0.16 ± 0.02
5 GeV electron trigger	0.9 ± 0.2	0.3 ± 0.2
5 GeV photon trigger	0.15 ± 0.02	0.2 ± 0.1
5 GeV electron and photon trigger	0.22 ± 0.05	0.3 ± 0.1
2 GeV electron trigger	0.62 ± 0.05	0.3 ± 0.1
2 GeV photon trigger	0.125 ± 0.008	0.18 ± 0.05
2 GeV electron and photon trigger	0.146 ± 0.008	0.24 ± 0.07

Table 7.3: Fraction of D* from beauty over all D*, for two values of p_T , for different samples.

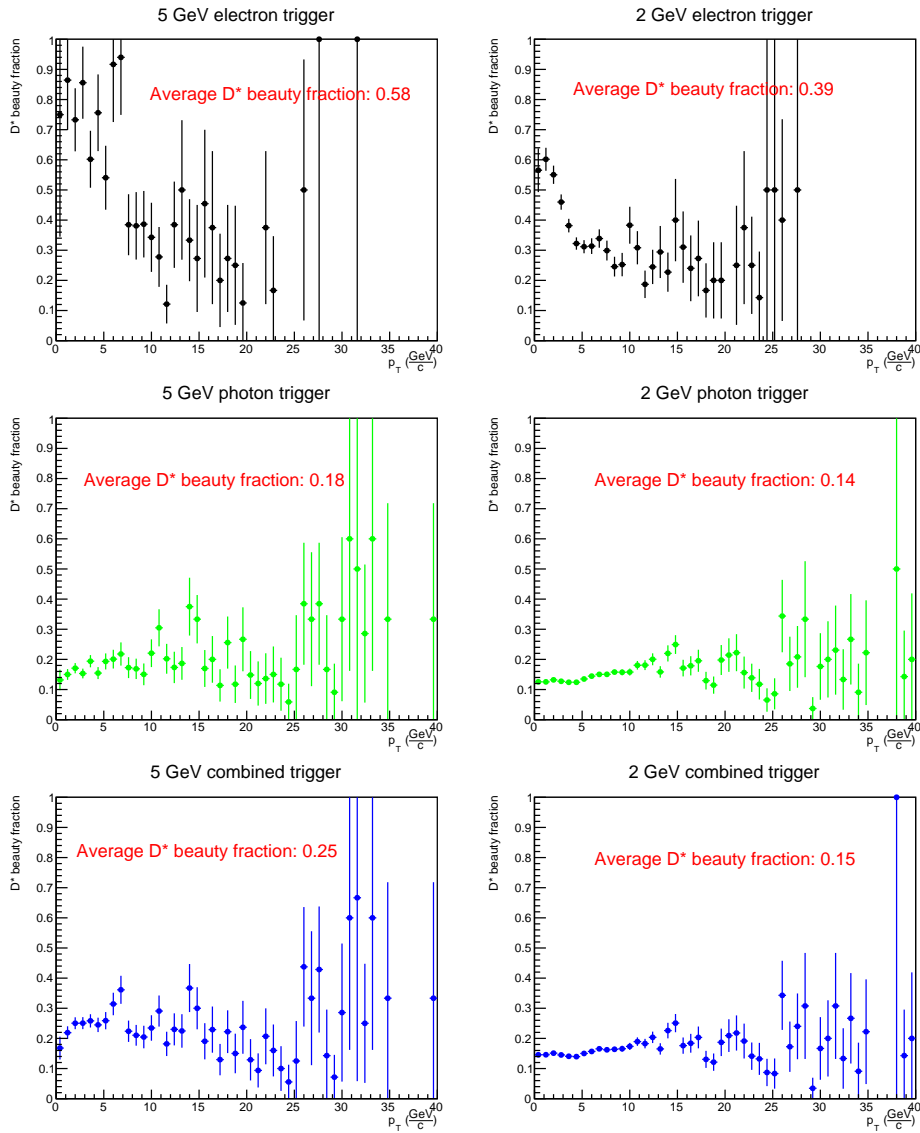


Figure 7.5: Fraction of D^* from beauty over all D^* , as a function of p_T , for different trigger samples.

7.4 B meson

In this last section, we shortly discuss the results of the trigger bias on the yield of B^0 and B^+ mesons. These mesons were not the main study area of this thesis, but they are of high importance for the on-going research of using HF quarks as probes for the QGP. In future studies, these results must be extended and further developed, to understand more of the trigger bias on the B meson yield.

In analyzing the trigger bias on the B meson yield, I combined the yield for all B^0 and B^+ mesons. In table 7.4 the amount of events, the yield and the average enhancement is given for B^0 and B^+ mesons combined, for different samples. The average enhancement is calculated by integration of the ϕ distributions in the minimum bias sample and the trigger sample, dividing those integrals and normalizing for the number of events in the samples.

We observe the electron triggers to greatly enhance the B meson yield. This enhancement is even bigger than the overall D^* yield enhancement, which is listed in table 6.1 in section 6.2. The photon triggers cause a relatively small enhancement.

Event sample	Meson yield	Overall enhancement factor
Minimum bias	$4.871 * 10^3 \pm 7 * 10^2$	-
5 GeV electron trigger	$2.07 * 10^3 \pm 5 * 10^1$	248 ± 5
5 GeV photon trigger	$3.38 * 10^3 \pm 6 * 10^1$	11.6 ± 0.2
5 GeV electron and photon trigger	$5.42 * 10^3 \pm 7 * 10^1$	18.0 ± 0.2
2 GeV electron trigger	$1.08 * 10^4 \pm 1 * 10^2$	121 ± 1
2 GeV photon trigger	$4.68 * 10^4 \pm 2 * 10^2$	6.29 ± 0.03
2 GeV electron and photon trigger	$5.62 * 10^4 \pm 2 * 10^2$	7.46 ± 0.03

Table 7.4: B^+ and B^0 meson yield and overall enhancement factor, for different samples. The mesons are found in $|\eta| < 0.9$.

Chapter 8

Conclusions and outlook

In the previous chapters I presented the results for the trigger bias on the D^* meson yield. In this chapter, I will summarize these results and draw conclusions, followed by recommendations for the implementation of one of the possible EMCal trigger in the ALICE detector. In the outlook, I will reflect on my thesis to evaluate the results and to investigate how they might be improved. Some additional plans and analysis methods are proposed for further refinement and expansion of the results of this thesis, to be done in future studies.

Conclusions

This thesis determined the bias of an EMCal trigger on the general D^* meson yield, on the D^* p_T distribution and on the beauty fraction. To achieve this, minimum bias collisions at $\sqrt{s} = 13$ TeV, simulated by Pythia, were analyzed and labelled as trigger events, if they met certain trigger conditions. Several different possible EMCal triggers have been considered, mainly the electron trigger and photon trigger, with two energy thresholds, 5 and 2 GeV. Subsequently, the D^* meson distributions were stored in different histograms, depending on their original event sample. Enhancement plots then gave insight into the trigger bias on the D^* yield as a function of p_T , ϕ or η .

In chapter 5 we have analyzed the functioning of the trigger and the properties and distributions of the trigger particles: electrons and photons. We observed that the high trigger energy thresholds, being 5 and 2 GeV, caused a drastic decrease in the amount of events in the trigger samples, compared to the amount in the minimum bias sample. From table 5.2 we know that a minimum bias sample of 100,000 events will yield only 1.72 events for the 5 GeV and 18.4 events for the 2 GeV electron trigger. According to table 5.4, for the photon trigger, the amount of events is more: 61 events for the 5 GeV and 1540 events for the 2 GeV photon trigger per 100,000 events.

Using an electron trigger and, to a lesser extent, a photon trigger, will greatly reduce the amount of events. If this will form an obstacle for the implementation of the trigger, depends on the frequency of the collisions taking place in ALICE and the frequency of the data taking. If the collisions are much more frequent than the maximum data taking speed, which causes ALICE to be able to capture less than 1 event in 100,000 collisions even without using a trigger, it will not be a problem. In this case, the implementation of the trigger will not change the total amount of events ALICE can capture in a given amount of time. However, if the data taking speed is higher, it can be a problem. Using a trigger will then cause a big decrease in the total amount of events which ALICE yields in a given amount of time, compared to the amount of events in the minimum bias sample. Although the D^* meson yield will be enhanced in the trigger sample, the trigger can still be useless if the amount of events is that much lower, that significantly less D^* will be found in the sample. Future studies should investigate this further, to give a definitive recommendation for the implementation of an EMCal trigger.

If it is the case that implementation of an EMCal trigger drastically reduces the amount of events, using the 2 GeV instead of the 5 GeV electron trigger can be an option. If even more events are to be produced, the combined (electron and photon) trigger will help. The photon trigger yields more events, and the combined trigger even more. The difference in D^* enhancement between the 2 GeV electron and 2 GeV combined trigger is not big enough to counter the loss of events, in the case of using an electron trigger. This is reflected in table 6.4, where we find that the combined trigger sample has in total more D^* mesons than the electron trigger sample.

Apart from this objection about the amount of events in the trigger sample, the 5 GeV electron trigger performs best in every category. The total enhancement factor for the D^* yield, listed in table 6.1, is 41 ± 1.3 for the 5 GeV and 30.5 ± 0.3 for the 2 GeV electron trigger. With the objective of maximizing D^* yield and reducing background, the 5 GeV electron trigger should therefore be implemented, followed by the 2 GeV electron trigger as the second best.

If the priority is to enhance high p_T D^* mesons, the 5 GeV electron trigger should again be implemented, because of the maximum enhancement factor of $1.3 * 10^3 \pm 3 * 10^2$ in the high p_T limit; followed by the 5 GeV electron and photon trigger, with a maximum enhancement factor of $2.1 * 10^2 \pm 35 * 10^1$. This electron and photon trigger combines the strong enhancement in the high p_T limit with more events.

For all trigger samples, we observe the highest D^* enhancement in the EMCal region: $110^\circ > \phi > 0^\circ$ and $|\eta| < 0.7$. In order to reduce the background compared to the D^* yield, and thus increasing the significance, the D^* analysis can incorporate new topological cuts: removing all data from outside the EMCal range. This will also remove signal, so it has to be de-

terminated experimentally if the increase in significance is worth the loss of signal.

In chapter 7 we discussed the trigger bias on the beauty fraction. In table 7.2, the average beauty fraction for the origin of D^* mesons is listed for all samples. The photon and combined trigger hardly have an effect on the beauty fraction, but the electron trigger does. The average beauty fraction for the 5 GeV electron trigger is 0.58 ± 0.03 , compared to 0.1077 ± 0.0003 for the minimum bias sample. Because the beauty quark is a particle of interest as a probe for the QGP, it makes sense to implement the 5 GeV electron trigger, on behalf of future studies about beauty-origin D^* mesons. In this trigger sample, already half of the D^* mesons will be from beauty, and a even higher fraction at low p_T (see figure 7.5).

Using an EMCAL trigger also greatly enhances the yield of B^0 and B^+ mesons. The 5 GeV electron trigger causes an average enhancement by a factor of 248 ± 5 . Although a full analysis of this enhancement falls outside the scope of this thesis, it promises good results for further studies.

In conclusion, the 5 GeV electron trigger performs best in the enhancement of the D^* yield, especially for D^* mesons with high values of p_T , and in boosting the beauty fraction, especially at low p_T . This trigger seems to be the most solid choice to implement in ALICE. However, a down side to the 5 GeV electron trigger is the great decrease in the amount of events. The consequences of this decrease still need to be determined, as it greatly depends on the frequency of collisions in the LHC and of event sampling in the ALICE detector.

Outlook

I will reflect on the analysis method used for this thesis to determine where the results might be improved or expanded. Also, the results of this thesis can be used to build upon in new studies, all directed at the improvement of our understanding of the QGP and QCD in general. Possible roads for future studies are mentioned in this section.

In chapter 3, I mentioned that in the data set used for this thesis, the interaction of the particles with the ALICE detector is not yet taken into account. To refine the results of this thesis, this interaction should be taken into account. This can be done by using the GEANT toolkit.

Because of the rare presence of energetic photons and electrons in pp collisions, the EMCAL triggers cause a decrease in the amount of events suited for being recorded in the same amount of collisions. The implications of the drastic decrease in events in the trigger sample compared to the minimum bias sample have to be explored further. The maximum sampling frequency of ALICE and the collision frequency have to be taken into account, in order to determine if this trigger induced decrease in the sampling frequency has

an effect on the total amount of events in a time period. If the resulting decrease is too strong, the trigger should probably not be implemented.

In this study, I included all D^* mesons in the analysis. However, only the subsequent decay channels $D^{*+} \rightarrow D^0 + \pi^+$ and $D^0 \rightarrow K^- + \pi^+$ are observable using current data analysis methods. This excludes D^* mesons with a semi-leptonic decay mode. But, perhaps precisely these decay modes, as they yield an electron, are the cause of the big enhancement of D^* meson yield as a result of the 5 GeV electron trigger. This has to be checked, as it would have major implications for the trigger performance. A possible method for the investigation of the effect of semi-leptonic decays modes of the D^* on the electron trigger bias, would be to exclude the D^* mesons, decaying through the semi-leptonic channel, and to observe the resulting trigger bias. Future studies can also try to include the semi-leptonic decay modes into the D^* analysis of the ALICE data sample.

The trigger bias on the B meson yield has been discussed briefly, but future studies need to improve these results.

The EMCal detector currently has a limited range in the spatial coordinates. The performance of the EMCal trigger would be improved if these ranges are extended to the range of the ALICE detector itself: all ϕ and $|\eta| < 0.9$.

Hopefully, if the results of this thesis lead to the implementation of the 5 GeV electron trigger, the D^* meson yield in ALICE pp collisions will indeed be enhanced. This opens new doors for determination of the nuclear modification factor, which encodes the interaction of the QGP with HF quarks. This experimental factor will then be compared with theoretical calculations, in order to select those theories in QCD that describe the QGP most accurately. The increase in the beauty fraction caused by the EMCal trigger also helps the study of pure beauty quark interaction with the plasma. By refining the analysis method, D^* mesons, exclusively coming from beauty decays, can be extracted from the collision data sets. This extraction is much easier if the beauty fraction will indeed increase as a result of the trigger, an effect we expect on basis of the presented results.

Appendix A

Kaon trigger

The results for the 5 and 2 GeV kaon triggers are presented here. The kaon trigger is in the thesis not included as a candidate EMCal trigger to be implemented, because hadrons do not produce a suitable signal in the EMCal. Specifically triggering on kaons would therefore not be an option. However, a specific kaon trigger could be designed in the future. Therefore, I studied the bias of the 5 and 2 GeV kaon trigger, as a starting point for future studies. We observe in all figures that the enhancement for the kaon trigger is comparable to the enhancement of the electron and photon trigger. The enhancement is slightly higher, especially in the EMCal ϕ and η acceptance range.

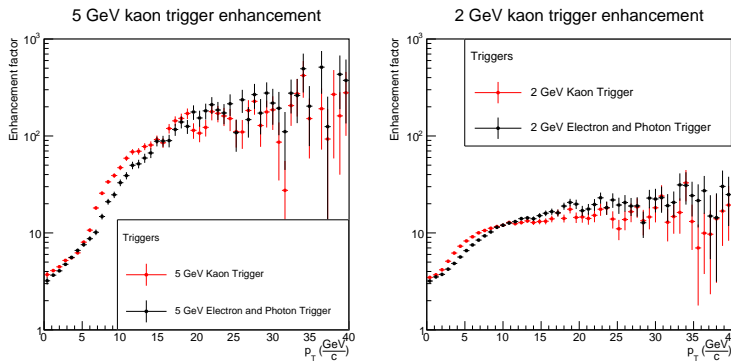


Figure A.1: D^* meson yield enhancement as a function of transverse momentum (p_T). The enhancement of the kaon trigger, and electron and photon trigger are compared, for the trigger energy threshold of 5 and 2 GeV.

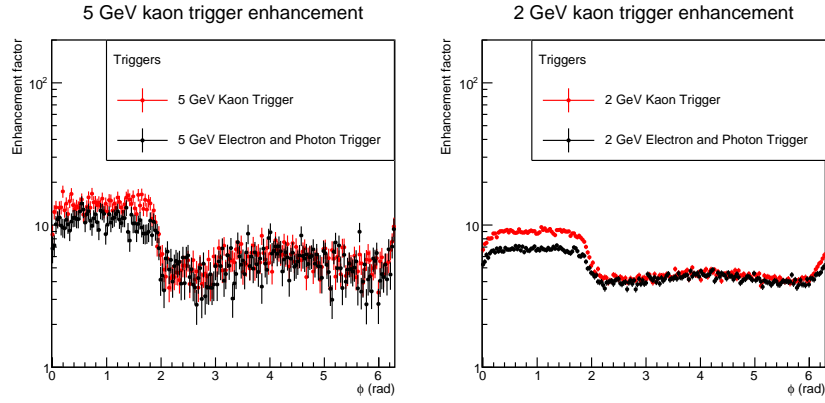


Figure A.2: D^* meson yield enhancement as a function of the azimuthal angle (ϕ). The enhancement of the kaon trigger, and electron and photon trigger are compared, for the trigger energy threshold of 5 and 2 GeV.

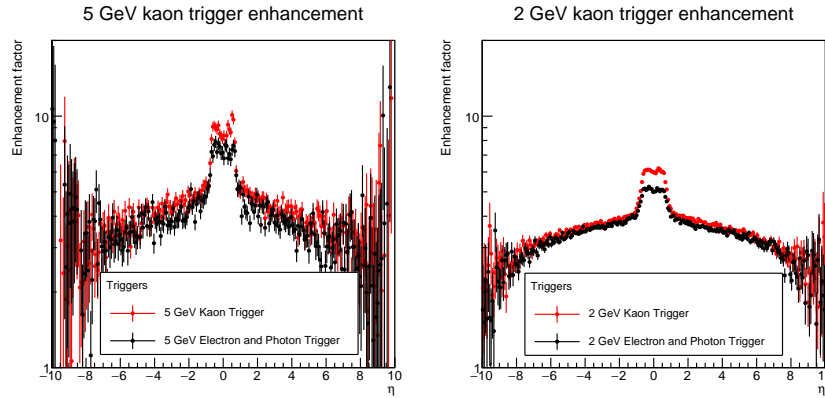


Figure A.3: D^* meson yield enhancement as a function of pseudorapidity (η). The enhancement of the kaon trigger, and electron and photon trigger are compared, for the trigger energy threshold of 5 and 2 GeV.

Bibliography

- [1] N. Serra, "Standard Model", UZH Physik-institut, Web: 29 Dec 2015, <http://www.physik.uzh.ch/groups/serra/StandardModel.html>.
- [2] J. Ellis and T. You, "Updated Global Analysis of Higgs Couplings", JHEP 1306(2013)103, [arXiv:1303.3879].
- [3] Y.K. Hsiao, C.Q. Geng, "Identifying Glueball at 3.02 GeV in Baryonic B Decays", Phys. Lett. B 727(2013)168-171 [arXiv:1302.3331].
- [4] "PANDA", RUG Hadronic and Nuclear Physics Research, Web: 29 Dec 2015, <http://www.rug.nl/kvi-cart/research/hnp/research/panda?lang=en>.
- [5] "The Nobel Prize in Physics 2004 - Advanced Information", Nobel-prize.org, Web: 30 Dec 2015 http://www.nobelprize.org/nobel_prizes/physics/laureates/2004/advanced.html.
- [6] J. Allday, "Quarks, Leptons and the Big Bang", CRC Press 2nd edition (2001).
- [7] J. Jowett, "LHC Report: plumbing new heights", CERN bulletin, Web: 4 January 2016, <https://cds.cern.ch/journal/CERNBulletin/2015/49/News%20Articles/2108943?ln=en>.
- [8] J. Jowett, "Lead-ion collisions: the LHC achieves a new energy record", CERN bulletin, Web: 4 January 2016, <https://cds.cern.ch/journal/CERNBulletin/2015/49/News%20Articles/2105084?ln=en>.
- [9] K. M. Walsh, "Tracking the Transition of Early-Universe Quark Soup to Matter-as-we-know-it", Brookhaven National Laboratory's Relativistic Heavy Ion Collider News, Web: 4 January 2016, <https://www.bnl.gov/rhic/news2/news.asp?a=4473&t=today>.
- [10] T. Song, C.M. Ko, S.H. Lee, "Quarkonium formation time in quark-gluon plasma", Phys. Rev. C 87(2013)034910, [arXiv:1302.4395].
- [11] M. Djordjevic, M. Gyulassy, "Where is the charm quark energy loss at RHIC?", Phys. Rev. B 560(2003)37-43, [arXiv:nucl-th/0302069].

- [12] A. Quadt, "Top quark physics at hadron colliders", *The Eur. Phys. Journal C - Particles and Fields*, 48,3(2006)835-1000.
- [13] R.S. de Rooij, "Prompt D^+ production in proton-proton and lead-lead collisions, measured at the CERN Large Hadron Collider", Ph.D. Thesis, Utrecht University (2013).
- [14] "ALICE", Irfu, Web: 4 January 2016, http://irfu.cea.fr/en/Phocea/Vie_des_labos/Ast/alltec.php?id_ast=2239.
- [15] L. Bryngemark, "Charged pion identification at high pT in ALICE using TPC dE/dx ", Conference proceedings of the 6th International Workshop High-pT physics at LHC (2011), [arXiv:1109.1896].
- [16] C. Lippmann, "Particle identification in ALICE: an extra boost in QGP studies - Part B", ALICE matters, Web: 4 January 2016, http://alicematters.web.cern.ch/?q=CL_PID2.
- [17] R. Bellwied, "ALICE EMCAL Physics Performance Report", Submitted to the U.S. Department of Energy for the ALICE EMCAL Collaboration(2010), [arXiv:1008.0413].
- [18] W. Riegler, "ALICE looks to the future", ALICE matters, Web: 4 January 2016, <http://alicematters.web.cern.ch/?q=ALICEfuture2013>.
- [19] "More details on the EMCAL", ALICE Public, Web: 4 January 2016, <http://alipub-dev.web.cern.ch/detectors/more-details-emcal>.
- [20] J. Beringer et al. (Particle Data Group), "Review of Particle Physics", *Phys.Rev.D* 86(2012)33.
- [21] J. Beringer et al. (Particle Data Group), "Review of Particle Physics", *Phys.Rev.D* 86(2012)885.
- [22] J. Beringer et al. (Particle Data Group), "Review of Particle Physics", *Phys.Rev.D* 86(2012)911.
- [23] Zeus Coll., "Measurement of charm fragmentation fractions in photo-production at HERA", *DESY* 13(2013)106.
- [24] J. Beringer et al. (Particle Data Group), "Review of Particle Physics", *Phys.Rev.D* 86(2012)1105.
- [25] J. Beringer et al. (Particle Data Group), "Review of Particle Physics", *Phys.Rev.D* 86(2012)911.